

Growth rate of self-sustained QED cascades induced by intense lasers

A. Mercuri-Baron,^{1,*} A. A. Mironov,^{1,*} C. Riconda,¹ A. Grassi,¹ and M. Grech²

¹*LULI, Sorbonne Université, CNRS, CEA, École Polytechnique,
Institut Polytechnique de Paris, F-75255 Paris, France*

²*LULI, CNRS, CEA, Sorbonne Université, École Polytechnique,
Institut Polytechnique de Paris, F-91128 Palaiseau, France*

It was suggested [A. R. Bell & J. G. Kirk, PRL **101**, 200403 (2008)] that an avalanche of electron-positron pairs can be triggered in the laboratory by a standing wave generated by intense laser fields. Here, we present a general solution to the long-standing problem of the avalanche growth rate calculation. We provide a simple formula that we apply to the case of the standing wave created by two circularly polarized lasers and demonstrate that it allows to predict the particle yield for the full range of intensity able to generate an avalanche. We account for the damping of the growth rate due to pair migration from the region of prolific generation and show that above a threshold in intensity, this effect is negligible. The growth rate calculation allows us to predict when abundant pair production will induce a back-reaction on the generating field due to plasma collective effects and screening. Our model shows excellent agreement with self-consistent PIC simulations and can be applied to study the generation of electron-positron pair avalanches in realistic field configurations to plan future experiments at ultra-high-intensity laser facilities.

I. INTRODUCTION

Relativistic electron-positron pair (or QED) plasma is a state of matter that is believed to be responsible for multiple striking and yet not fully explained astrophysical phenomena. It can be generated in the vicinity of compact objects such as black holes [1, 2] or neutron stars [3] and pulsars [4–6]. Interactions with such QED plasma can be the source of prominent hard cosmic radiation in Gamma Ray Bursts and in bright gamma flashes from relativistic jets [7–10]. Abundant production of e^-e^+ pairs can take place in cascade processes developing in polar caps of a rotating compact star [2, 11]. This mechanism opens a path to explain the nature of radio-pulsar emission [12, 13] and the source for plasma populating the magnetosphere of a star and the magnetic reconnection layer [14–16].

A laboratory study of dense relativistic electron-positron pair plasma would facilitate a breakthrough in our understanding of the impact of QED effects in astrophysical phenomena. However, the generation of such plasma appears to be exceptionally challenging [17, 18]. The first observation of a neutral e^-e^+ plasma state was reported only a few years ago [19], and the first investigation of collective behaviour was done very recently [20]. Still, in both cases, the density of electrons and positrons, generated via the Bethe-Heitler process, barely reached the value high enough to form a plasma.

A prospective path to obtaining e^-e^+ plasma in the laboratory lies in using super-strong electromagnetic (EM) fields, for example, generated with ultra-high intensity lasers [21–25]. When interacting with elementary

particles, such fields can induce a wide variety of nonlinear strong-field QED (SFQED) phenomena by sharing $N \gg 1$ soft photons γ_L with e^\pm [26–30]. The two leading order effects are the nonlinear inverse Compton scattering (for brevity, Compton emission) $e^\pm + N\gamma_L \rightarrow e^\pm + \gamma$ and the nonlinear Breit-Wheeler pair production¹ $\gamma + N\gamma_L \rightarrow e^- + e^+$. The strong-field QED treatment of these processes is essential when the field experienced by a relativistic particle in its rest frame² is comparable to the critical field of QED $E_S = m^2 c^3 / (e\hbar)$, where m and $-e$ are the electron mass and charge, respectively. Sequential Compton emissions and Breit-Wheeler pair productions can lead to cascades.

Cascades can be generated as *shower-type* events by incident high-energy particles in a strong field [31–33]. According to the estimates [25, 34, 35], the shower particle yield is defined by the energy input from the incident bunch. The configuration envisioned in this scheme is similar to Bethe-Heitler process-based setups [36], with the only difference that in the former the field is provided by high-Z nuclei. In the classical limit (namely, in weak fields or at low particle energy), the Compton emission describes classical radiation by a charge, while the Breit-Wheeler process is suppressed [37]. This naturally limits the shower multiplicity.

Strong EM fields can induce a different phenomenon originally predicted by Bell & Kirk [38]: electron-seeded *avalanche-type* (or self-sustained) QED cascades. They can be triggered by low-energy electrons injected into the strong field region (illustrated in Fig. 1). The initial and secondary charged particles experience ongoing acceleration by the field, which restores their energy in between

* These two authors contributed equally.
anthony.mercuri@protonmail.com
mironov.hep@gmail.com

¹ For brevity, we omit the word ‘nonlinear’ throughout the paper when referring to both these processes.

² For a photon of frequency ω_γ in the laboratory frame, the analogous frame can be defined as the one where $\hbar\omega'_\gamma = mc^2$.

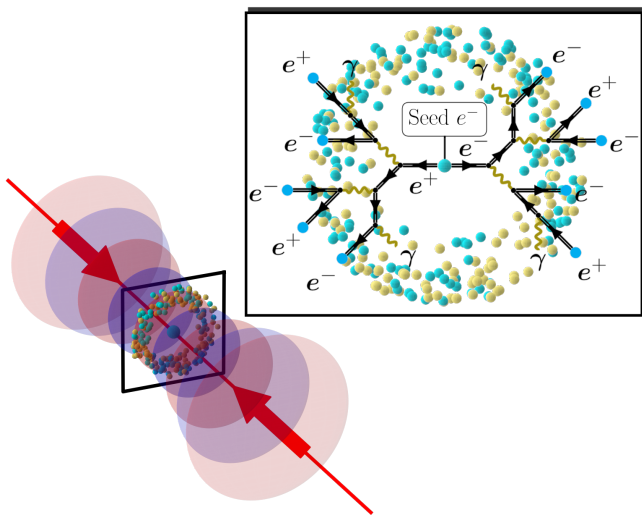


Figure 1. Schematic representation of an avalanche-type cascade. Blue and yellow balls show e^\pm and γ , respectively. The initial electron is injected into the focus of a CP standing wave formed by two counterpropagating laser beams. The field at electric antinode accelerates initial and secondary e^\pm in the direction transverse to the optical axis. This acceleration renders the onset and further development of the cascade with prolific production of e^+e^- pairs.

hard photon emissions, therefore sustaining the cascade. In an avalanche triggered even by few seed electrons, the number of produced e^-e^+ pairs can rapidly exponentiate with time and field strength [39, 40]. The process is accompanied by a bright gamma-flash [41]. Such cascades induced by lasers can hence mimic the processes developing in the polar caps of rotating neutron stars [2, 11, 12].

The avalanche-type cascades can onset in alternating electric fields that are strong enough [42]. The suitable configurations include electric antinodes of standing waves formed by two counterpropagating laser beams of an optical frequency and circularly [39, 43–45] or linearly [46, 47] polarized; a multi-beam setup [48, 49] and a dipole wave as its limiting case [41]; a single ultra-intense beam focused in vacuum [42] or reflected from a plasma mirror [50]; irradiation of a solid [51–53], a plasma slab [54, 55], or a gas target [56, 57], vortex laser pulses [58] (for a more detailed review see Refs. [26–28]). Simulations show that an electron-positron plasma can be generated in a single laser shot and reach a high density demonstrating collective effects [22, 59–61] or even screening the field [45, 51, 62–64].

Simulations for the mentioned setups show that the intensity required for initiating an electron-seeded avalanche-type cascade is of the order of 10^{24} W/cm² for a femtosecond optical laser pulse. Intensities approaching this value are anticipated to be within the reach of the new generation of multi-petawatt laser facilities, such as Apollon [65], ELI-Beamlines [66], CoReLS [67], and more worldwide [68–72]. The record intensity of $\approx 10^{23}$ W/cm² was recently reported [73], and increasing efforts

are invested to reach 10^{24} – 10^{25} W/cm² in the near future [74–77].

In this work, we address two general questions: (i) What is the scaling of the particle yield with the field strength in an avalanche-type cascade developing in a realistic field configuration? and (ii) What are the requirements to reach plasma densities in such cascades? Assuming that initial electrons are already injected in the strong field, the cascade development splits into the onset and exponential phases, with the majority of particles produced in the latter. While the general onset conditions seem clear from the theoretical viewpoint [42], a universal model for the exponential growth rate of particles is lacking.

Most of the progresses in the theory of avalanche-type cascades were made for a uniform rotating electric field (for brevity, we refer to it as ‘rotating E -field’). This field corresponds to the electric antinode (E -antinode) of a circularly polarized (CP) standing wave formed by two counterpropagating laser beams. It was initially estimated in Refs. [40, 43] that cascades can develop in fields of the order $\sim \alpha E_S$, which corresponds to intensity $\sim 10^{25}$ W/cm² for an optical laser field. Here, $\alpha = e^2/(4\pi\epsilon_0\hbar c) \approx 1/137$ is the fine structure constant. Yet, simulations show [26, 45] that cascades can be triggered at fields lower by an order of magnitude, and the resulting growth rate of e^-e^+ pairs matches the prediction of Refs. [40, 43] only at very high fields. Subsequent works [45, 46, 63] provide some phenomenological models improving this estimate in (relatively) low- and high-field regimes, and Ref. [78] in the mid-range. However, these results do not provide a general dependence on the field strength valid in the full range and are limited to the model of a rotating E -field.

Another effect that is not treated in the above-mentioned models and will be discussed in this paper, is particle migration. In realistic field configurations, particles can escape from the strong field region, e.g. as observed at the E -antinode in a standing wave [79, 80]. This proves important in the low field regime where migration can reduce the overall e^-e^+ pair yield [47].

Under the semiclassical approximation, the kinetic approach provides a general basis for describing the particle distribution evolution in cascades [43, 62, 81, 82]. Indeed, common numerical approaches solve kinetic equations in the Monte-Carlo scheme or particle-in-cell codes. The latter allows accounting for plasma effects by consistent treatment of the Vlasov and Maxwell equations [83]. Notably, a kinetic description also allows to account for spin effects [84–86].

We adopt the kinetic approach for an ab-initio derivation of the particle growth rate expression in an avalanche-type cascade and rigorously define the approximations in use. Moreover, this approach allows us to theoretically account for particle migration and highlight its effect on the growth rate. We focus on cascades developing in the CP standing wave configuration, however, we believe that our considerations can be generalised to the

wide class of fields considered in Ref. [42].

We leave aside the nontrivial question of injecting the initial electrons [87, 88] and assume that they are located in the strong field region. Let us mention that seeding can be implemented by using a high-energy electron bunch [44, 89], ionizing a jet of high-Z atoms [56], or solid targets [21, 52]. At extreme fields, seed electrons can be created due to Schwinger e^-e^+ pair production, which can become feasible due to the large volume of the focal spot [49, 90]. As we aim at finding the field scaling of the avalanche-type cascade growth rate, for simplicity, we omit the Schwinger effect, as well as spin contribution in the current work.

The paper is organized as follows. At the beginning of Sec. II we introduce our notations and give an overview of the approximations in use. In Sec. II A we present the probability rates of the basic processes. In Sec. II B, following Ref. [42], we postulate the semiclassical short-time dynamics of a single electron in a general accelerating field. This is then used in Sec. II C to define the characteristic time between Compton emissions for the electron and to find the key parameters entering in the emission process. In Sec. II D we discuss the related asymptotic limits. Section III is devoted to our major result, namely, the master equations for the particle numbers and the general formula for the avalanche-type cascade growth rate (taking into account particle migration) in Sec. III A, the effective model for the growth rate in Sec. III B, and its low- and high-field limits in Sec. III C. In Sec. IV, we apply our model to study avalanches developing in a CP standing EM wave at relatively low- and mid-range fields and test the model against simulations performed with the PIC-QED code SMILEI [91]. Section IV A contains details about the numerical setup and data analysis, while in Sec. IV B discuss the physical results and validate our model. Section V A continues this discussion for high fields, and in Sec. V B we compare our results with previous works. In Sec. VI we apply our model to identify the field parameters at which the plasma state can be reached in avalanche-type cascades in a rotating E -field and test the model against PIC simulations. In Sec. VII we summarise and discuss our results.

II. PARTICLE DYNAMICS IN A CASCADE

The interaction of a relativistic particle (electron, positron, or photon) with a strong EM field can be characterized by two parameters. First, by the parti-

cle Lorentz factor γ_e for e^\pm or by the normalized energy $\chi_\gamma = \hbar\omega_\gamma/mc^2$ for a photon with frequency ω_γ . Second, by the invariant quantum dynamical parameter combining the electron³ or photon momentum $\mathbf{p}_{e,\gamma}$ and the elec-

³ Hereinafter, we treat electrons and positrons identically, and for brevity refer to both as just ‘electrons’ unless mentioned explicitly.

tric and magnetic field components \mathbf{E} and \mathbf{B} :

$$\chi_{e,\gamma} = \frac{1}{E_S} \sqrt{(\gamma_{e,\gamma} \mathbf{E} + c \mathbf{u}_{e,\gamma} \times \mathbf{B})^2 - (\mathbf{u}_{e,\gamma} \cdot \mathbf{E})^2}, \quad (1)$$

where $\mathbf{u}_{e,\gamma} = \mathbf{p}_{e,\gamma}/(mc)$. For an electron, χ_e equals the rest frame field strength in the units of the QED critical field $E_S = m^2 c^3 / (e \hbar)$.

Parameter (1) allows to assess when the quantum effects in the interaction of a particle with an external EM field need to be considered. They become important at $\chi_{e,\gamma} \gtrsim 1$. As mentioned in the introduction, we consider two leading order field-induced effects: the nonlinear Compton emission and nonlinear Breit-Wheeler process. In this work, we adopt the probability rates for these processes within the locally constant field approximation (LCFA) [37, 92–94]. It implies that the rates depend only on the field strength at the local position of the incoming relativistic particle, and the field is close to the constant crossed EM field in the particle reference frame [26, 37]. Furthermore, in a quantum process, the produced and scattered particles propagate collinearly to the incoming one.

It should be noted, that the LCFA breaks if one of the particles in the process is nonrelativistic or the transverse field seen by the particle is relatively low [95] (see more discussions in Refs. [96–103]). However, the LCFA is reasonable for modeling avalanche-type cascades, as under optimal conditions for their onset, such events are rare and also do not contribute to the cascade particle growth rate [42, 95].

A. Photon emission and pair creation probability rates

The differential probability rate for an electron with the Lorentz factor γ_e and quantum parameter χ_e to emit a photon with energy within the interval $mc^2 \times (\gamma_\gamma, \gamma_\gamma + d\gamma_\gamma)$ is given by

$$\frac{dW_{\text{cs}}(\gamma_e, \chi_e, \gamma_\gamma)}{d\xi} = \frac{1}{\sqrt{3}\pi} \frac{\alpha}{\tau_C \gamma_e} \left[\left(1 - \xi + \frac{1}{1 - \xi} \right) K_{2/3}(\mu) - \int_\mu^\infty ds K_{1/3}(s) \right], \quad (2)$$

where $\tau_C = \hbar/(mc^2)$ is the Compton time, and we defined $\mu = 2\xi/[3\chi_e(1 - \xi)]$, $\xi = \gamma_\gamma/\gamma_e \equiv \chi_\gamma/\chi_e$. K_n are the n -th order modified Bessel functions of the second kind. Note that the χ -parameter is conserved, $\chi_e = \chi_\gamma + \chi'_e$, where χ'_e corresponds to the scattered electron. The differential probability rate for a photon with γ_γ and χ_γ to produce a pair

of e^-e^+ , so that either e^- or e^+ gets energy within the interval $mc^2 \times (\gamma_e, \gamma_e + d\gamma_e)$, reads:

$$\frac{dW_{\text{BW}}(\chi_\gamma, \gamma_\gamma, \gamma_e)}{d\zeta} = \frac{1}{\sqrt{3}\pi} \frac{\alpha}{\tau_C \gamma_\gamma} \left[\left(\frac{\zeta}{1-\zeta} + \frac{1-\zeta}{\zeta} \right) K_{2/3}(\mu') - \int_{\mu'}^{\infty} ds K_{1/3}(s) \right], \quad (3)$$

where $\mu' = 2\zeta/[3\chi_\gamma(1-\zeta)]$, $\zeta = \gamma_e/\gamma_\gamma \equiv \chi_e/\chi_\gamma$, and $\chi_\gamma = \chi_e + \chi_e'$. Here, χ_e and χ_e' correspond to the electron and positron.

The total probability rates $W_{\text{CS}}(\gamma_e, \chi_e)$, $W_{\text{BW}}(\chi_\gamma, \gamma_\gamma)$ are obtained by integrating out the final particle energies or, equivalently, ξ and ζ :

$$W_{\text{CS}}(\gamma_e, \chi_e) = \int_0^1 \frac{dW_{\text{CS}}(\gamma_e, \chi_e, \gamma_\gamma)}{d\xi} d\xi, \quad (4)$$

$$W_{\text{BW}}(\chi_\gamma, \gamma_\gamma) = \int_0^1 \frac{dW_{\text{BW}}(\chi_\gamma, \gamma_\gamma, \gamma_e)}{d\zeta} d\zeta \quad (5)$$

In the asymptotic case, they can be simplified:

$$W_{\text{CS}}(\gamma_e, \chi_e) \approx \frac{\alpha}{\tau_C \gamma_e} \times \begin{cases} 1.44 \chi_e, & \chi_e \ll 1, \\ 1.46 \chi_e^{2/3}, & \chi_e \gg 1, \end{cases} \quad (6)$$

$$W_{\text{BW}}(\chi_\gamma, \gamma_\gamma) \approx \frac{\alpha}{\tau_C \gamma_\gamma} \times \begin{cases} 0.23 \chi_\gamma e^{-\frac{8}{3\chi_\gamma}}, & \chi_\gamma \ll 1, \\ 0.38 \chi_\gamma^{2/3}, & \chi_\gamma \gg 1. \end{cases} \quad (7)$$

The probability rates and the product spectrum width grow with the χ -parameter of the incoming particle (if the Lorentz factor is fixed). On the other hand, the χ -parameter is shared among the products in each quantum event, so its value decreases for subsequent particle generation. As a result, if a high-energy particle in a laser field triggers a cascade, at some point it will stop unless the χ -parameter increases again during the particle propagation in between the quantum events [33, 44]. For this reason, the multiplicity of shower-type cascades is defined by the energy of incident particles, as χ decreases for each generation of secondary particles.

B. χ_e time dependence in accelerating fields

The key idea of the avalanche-type cascade mechanism is that in between emission events electrons are re-accelerated by the field, which restores a high value of χ_e . Then the cascade will be sustained as long as particles experience a strong field. The mean free path time of an electron or a photon in an external EM field can be estimated as the inverse total probability rate $W_{\text{CS}, \text{BW}}^{-1}$. Let ω^{-1} be the time scale of the field variation. For a particle in a prolific cascade, we expect that $\omega W_{\text{CS}, \text{BW}}^{-1} < 1$ [38, 40], i.e. multiple quantum events take place during a field cycle. The cascade overall properties, such as the particle number growth rate and spectra, are defined by the single-particle χ_e evolution at the time scale $\omega t \ll 1$.

Let us consider an electron (seed or secondary) in a strong accelerating field. The evolution of γ_e and χ_e at

$\omega t \ll 1$ can be written explicitly as proposed in Ref. [42]:

$$\gamma_e(t) \simeq \frac{eEt}{mc}, \quad (8)$$

$$\chi_e(t) \simeq \frac{\epsilon^2 \omega_{\text{eff}}^2 t^2}{E_S^2 \tau_C}, \quad (9)$$

where, in simple terms, $\epsilon \propto E$ can be regarded as the electric field strength E experienced by the electron at its initial position, and the effective frequency $\omega_{\text{eff}} \propto \omega$ represents the time and length scale of the field variation. The full expressions for ϵ and ω_{eff} are presented in Appendix A. Let us note here that ϵ is Lorentz-invariant and defined as the electric field in the frame where the electric and magnetic components are parallel or one of them vanishes [37, 104]. The effective frequency ω_{eff} is defined via the local field derivatives and vanishes for a constant field. The combination $\omega_{\text{eff}}^2 t^2$ is also invariant.

Equations (8) and (9) are general for a wide class of EM fields, and are valid under the following assumptions:

- (i) *the particle dynamics is semiclassical*, namely, photons propagate along straight lines and electron motion satisfies the Lorentz equations. This holds for subcritical fields, $E \ll E_S$, which is relevant for laser beams and astrophysical applications;
- (ii) the field components at the initial position of the electron satisfy the condition $E > cB$. We refer to such configurations as to *fields of electric type*.
- (iii) by the time moment of emission $W_{\text{CS}}^{-1} \ll \omega^{-1}$, the *energy gained by the electron from the field is high* compared to its initial energy (i.e. particles rapidly ‘forget’ their initial conditions).

Then the electron trajectory can be approximated and substituted in Eq. (1), which results in Eqs. (9). We provide some details about the derivation in Appendix A, which follows Ref. [42].

It is important to note that fields with $E = cB$ or $E < cB$ (so-called null and magnetic-type fields) do not fulfil the conditions for sustaining the cascade. In both cases, χ_e does not increase as the electron propagates, and therefore they are not favourable for the avalanche-type cascade development⁴.

⁴ A remarkable exception is cascading in pulsar polar caps where curved magnetic lines extend over very large distances. The photons resulting from curvature radiation experience increasing transverse magnetic field as they propagate, and hence χ_γ grows, which in turn can supply the cascade development [11–13].

One of the suitable configurations is the electric antinode of a standing wave formed by two counter-propagating circularly polarized (CP) laser beams [39, 40, 43, 45, 46, 52, 53, 62], where the magnetic field is absent and the electric component is close to a uniform rotating electric field:

$$\mathbf{E} = E_0 [\cos(\omega t)\hat{\mathbf{x}} + \sin(\omega t)\hat{\mathbf{y}}], \quad (10)$$

with $E_z = 0$, $\mathbf{B} = 0$. In this case, one has $\epsilon = E_0$, $\omega_{\text{eff}} = \omega/2$, and Eqs. (8)-(9) read [40, 43, 62]:

$$\gamma_e(t) \simeq \frac{eE_0 t}{mc}, \quad \chi_e(t) \simeq \frac{E_0^2 \omega t^2}{2E_S^2 \tau_C}. \quad (11)$$

C. Characteristic γ_e and χ_e at emission

Once the evolution of χ_e for the accelerated electron is determined, it can be used to calculate the time instant of photon emission and the corresponding values of γ_e and χ_e at this moment. These quantities identify whether the electron-seeded cascade can onset [42] and the particle growth rate (as we will show in Sec. III).

In a prolific avalanche-type cascade, the number of particles rapidly exponentiates with time and therefore is sensitive to small variations of the parameters that enter in the growth rate. For this reason, in our model, we go beyond the simple estimate for the electron mean free path time as the inverse emission rate, W_{cs}^{-1} . Let us introduce the characteristic time of electron propagation between photon emissions t_{em} :

$$\int_0^{t_{\text{em}}} W_{\text{cs}}(t') dt' := 1, \quad (12)$$

where $W_{\text{cs}}(t) = W_{\text{cs}}(\gamma_e(t), \chi_e(t))$, and $\gamma_e(t)$ and $\chi_e(t)$ are given by Eqs. (8)-(9). It is convenient to introduce the corresponding characteristic values:

$$\gamma_{\text{em}} = \gamma_e(t_{\text{em}}), \quad \chi_{\text{em}} = \chi_e(t_{\text{em}}), \quad (13)$$

obtained by substituting t_{em} into Eqs. (8)-(9). As we will show, the cascading regime is characterised by χ_{em} . Let us stress here, that t_{em} , γ_{em} , and χ_{em} depend only on the field parameters via ϵ and ω_{eff} :

$$\epsilon, \omega_{\text{eff}} \mapsto \{t_{\text{em}}, \gamma_{\text{em}}, \chi_{\text{em}}\}. \quad (14)$$

In view of Eqs. (8)-(9), χ_{em} can be chosen as an independent variable instead of t_{em} (assuming that ϵ and ω_{eff} are nonzero). In particular, by inverting Eq. (9) and passing to the corresponding variable in Eq. (12), we can rewrite the latter in the Lorentz-invariant form:

$$\int_0^{\chi_{\text{em}}} d\chi \frac{\tau_C W_{\text{cs}}(1, \chi)}{2\alpha\chi} = \frac{\epsilon}{\alpha E_S}, \quad (15)$$

where we moved the physical parameters to the RHS, and the integrand in the LHS is a dimensionless special function of χ (note that the dependence on α cancels in the LHS as $W_{\text{cs}} \propto \alpha$). This expression defines χ_{em} (that is Lorentz invariant) in the electron reference frame. As one may notice, χ_{em} is independent of ω_{eff} .

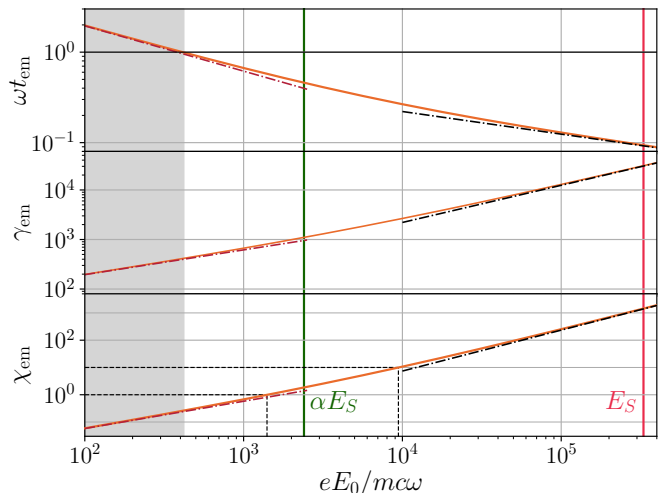


Figure 2. The emission characteristic time t_{em} and the corresponding values γ_{em} and χ_{em} [see Eqs. (12)-(13)] as functions of E_0 for an electron-seeded cascade in a uniform rotating electric field (solid lines). The dot-dashed lines show the low- and high-field asymptotic behavior. The short-time dynamics model given in Eqs. (8)-(9) is valid in the unshaded area, where $\omega t_{\text{em}} < 1$. Thin dashed lines in the bottom panel show the field strength at which $\chi_{\text{em}} = 1$ and 10. The vertical green line $E_0 = \alpha E_S$ corresponds to $eE_0/(mc\omega) \approx 2400$ and the vertical red line $E_0 = E_S$ — to $eE_0/(mc\omega) \approx 3.3 \times 10^5$. The field rotation frequency ω corresponds to the wavelength $\lambda = 0.8\mu\text{m}$.

D. Weak and high field regimes of photon emission by accelerated electrons

Formula (15) establishes the general functional dependence $\chi_{\text{em}} = \chi_{\text{em}}(\epsilon/\alpha E_S)$. At $\chi_{\text{em}} \ll 1$ or $\gg 1$ Eq. (15) simplifies, as we can use the asymptotic expressions (6) for W_{cs} to approximate the integral. The result sets the direct correspondence

$$\chi_{\text{em}} \ll 1 \iff \epsilon \ll \alpha E_S, \quad (16)$$

so that

$$\chi_{\text{em}} \simeq \begin{cases} 1.39 \frac{\epsilon}{\alpha E_S}, & \epsilon \ll \alpha E_S, \\ 0.87 \left(\frac{\epsilon}{\alpha E_S} \right)^{3/2}, & \epsilon \gg \alpha E_S. \end{cases} \quad (17)$$

Relation (16) defines the weak and strong field regime of an avalanche-type cascade, with αE_S being the threshold.

Analogously to Eq. (17), we can also calculate the asymptotic behavior of t_{em} and γ_{em} . The resulting expressions with the full numerical coefficients are presented in Appendix B.

For illustration, in Fig. 2, we show the dependence of t_{em} , γ_{em} , and χ_{em} on the field strength for an electron accelerated by a uniform rotating electric field [Eq. (10)]. As t_{em} and χ_{em} are defined via the full expression (4) for

W_{cs} [see Eqs. (12), (15)], we calculate them by numerical integration. We confirm that our initial assumption $\omega t_{\text{em}} < 1$, required in Eqs. (8)-(9), is met in a wide range of E_0 and improves with a growing field strength. We also plot the asymptotic expressions for χ_{em} [given in Eq. (17)], as well as for t_{em} and γ_{em} (see Appendix B). As expected, the low and high field asymptotics set in at $E_0 \ll \alpha E_S$ and $\gg \alpha E_S$, respectively. Finally, let us note that in the transition regime $E_0 \sim \alpha E_S$, χ_{em} takes the value $1 \lesssim \chi_{\text{em}} < 10$. This interval will also correspond to the transition between the models for the cascade growth rate, which we present in the following Section.

III. STEADY-STATE PARTICLE GROWTH RATE OF A CASCADE IN A GENERAL FIELD

Let us now address the evolution of the particle number in an avalanche-type cascade and its scaling with the field strength, which is the central question of this work. We consider a field that meets the validity conditions for Eqs. (8), (9) in a localized region. In the context of a standing EM wave, this can be an electric antinode, with the limitation that particles can be expelled (or 'migrate') from the region of strong electric field. In this section, we derive the master equations for the particle number evolution and take this effect into account.

We show explicitly by an ab initio calculation that the master equations, proposed phenomenologically in the absence of migration in Ref. [46] and later used in Refs. [45, 61], are exact if the photon emission and pair creation rates entering in the equations are calculated by averaging over the particle distributions. However in general the analytic expression for the distribution functions and hence the rates are unknown. Here, we propose an approximation for the latter based on the small-time electron dynamics discussed in the previous Section. As a result, this allows us to solve the master equations and find the explicit scaling of the cascade growth rate with the field strength.

A. Growth rate in the steady state

The onset stage of the avalanche-type cascade is highly nonstationary. The seed particle distribution rapidly evolves as new e^-e^+ pairs and photons are produced. Provided that the particle yield is high at the scale of field duration, the particle energy quickly averages out as the cascade develops. The cascade can enter the so-called (quasi-)steady state, in which the energy distribution relaxes to a stationary function [43, 45]. We assume that the system quickly reaches this state (which we further confirm with numerical simulations), in which the particle number grows exponentially at a constant rate. However, depending on the field strength, the relaxation can take up to multiple field periods in time. Hence, particles can migrate from the strong-field area

due to the field gradient at a rate ν , which in turn can reduce the overall particle production rate. This should be accounted for in the cascade models when applied to realistic field configurations such as standing EM waves or focused laser pulses.

The steady-state master equations for the number of generated pairs N_p and photons N_γ can be derived by using the kinetic approach, as we show in Appendix C:

$$\frac{dN_p}{dt} = W_{\text{cr}}N_\gamma - \nu N_p, \quad (18)$$

$$\frac{dN_\gamma}{dt} = -W_{\text{cr}}N_\gamma + 2W_{\text{rad}}N_p, \quad (19)$$

where $W_{\text{rad,cr}}$ are the effective constant rates of photon emission and pair creation, respectively, and the migration rate ν represents the average stationary flow of particles leaving the cascading region. These equations are *exact*, and $W_{\text{rad,cr}}$ result from averaging $W_{\text{cs,bw}}(\gamma, \chi)$ over the steady-state particle distributions $f_{p,\gamma}(\gamma, \chi)$:

$$W_{\text{rad,cr}} = \langle W_{\text{cs,bw}}(\gamma, \chi) \rangle. \quad (20)$$

In the derivation of Eqs. (18)-(20), we rely only on the semiclassical approximation and the LCFA.

The master Eqs. (18)-(19) implicitly incorporate the emission and pair creation spectra without additional approximations about their shape. The analytical description of the particle distribution evolution in a cascade requires convoluting the differential probability rates from Eqs. (2), (3) with the distribution functions in the momentum space $f_{p,\gamma}(\mathbf{p}, t)$. However, when we consider the particle numbers $N_{p,\gamma}(t)$, the cascade yield is determined only by the effective total rates (20). We present our derivation in Appendix C for a cascade developing in the E -antinode of a CP standing wave-like configuration, but it can be generalized to other field configurations that allow a steady state.

Eqs. (18)-(19) can be solved by the substitution $e^{\lambda t}$, resulting in two eigenvalues λ . As one of them, denoted by Γ , is positive, the particle number increases exponentially with time, $N_{p,\gamma}(t) \sim e^{\Gamma t}$, and the growth rate reads:

$$\Gamma[W_{\text{rad}}, W_{\text{cr}}] = \frac{W_{\text{cr}} + \nu}{2} \left[\sqrt{1 + \frac{4W_{\text{cr}}(2W_{\text{rad}} - \nu)}{(W_{\text{cr}} + \nu)^2}} - 1 \right]. \quad (21)$$

For a given EM field configuration, $W_{\text{rad,cr}}$ and ν depend on the field parameters, and hence the growth rate Γ .

A calculation of the effective rates $W_{\text{rad,cr}}$ and ν requires averaging over the particle distribution functions $f_{p,\gamma}$. As their analytic expressions are unknown even in the simplest case of the rotating electric field configuration, they can be extracted from numerical simulations. Alternatively, they can be estimated under additional approximations, as, for example, was done for $W_{\text{rad,cr}}$ in Refs. [40, 43, 45, 46, 63]. The rate of migration in a region of size $\sim 2\pi c/\omega$ can be estimated as $\nu \sim \omega/(2\pi)$. For higher precision calculations we use the numerical

data. Anticipating further discussion in Section IV, let us note here that ν weakly scales with the field strength. In contrast to this, $W_{\text{rad,cr}}$ strongly depend on the field parameters. In what follows, we propose a refined analytical model for $W_{\text{rad,cr}}$, which is valid in a wide class of EM field models.

B. Effective emission and pair creation rates and model for Γ

Let us approximate the effective rates of photon emission W_{rad} and pair creation W_{cr} . We adapt the general idea of Ref. [40], where it was proposed to estimate W_{rad} at the characteristic γ_e and χ_e gained by e^- in a uniform rotating field before the instant of emission. We go beyond this simple estimate as we (i) consider a general accelerating field [in the context of Eqs. (8)-(9) validity], (ii) use the refined expressions for γ_{em} and χ_{em} to describe the radiating e^- , which we propose in Section II C, and (iii) treat electrons and photons differently depending on the field strength.

To evaluate the effective emission rate W_{rad} by an electron contributing to an avalanche-type cascade, we plug the characteristic values for $\gamma_e \sim \gamma_{\text{em}}$ and $\chi_e \sim \chi_{\text{em}}$ at the time of emission [see Eqs. (12)-(13)] into the full probability rate for the Compton emission [Eq. (4)]:

$$W_{\text{rad}} \simeq W_{\text{cs}}(\gamma_{\text{em}}, \chi_{\text{em}}). \quad (22)$$

Note that in a strong field such that $\chi_{\text{em}} \gg 1$, the field dependence of the emission probability rate can be written explicitly [see also Eq. (B6) in Appendix B]:

$$W_{\text{cs}}(\chi_{\text{em}} \gg 1) \approx 1.43 \alpha \sqrt{\frac{\omega_{\text{eff}}}{\tau_C}} \left(\frac{\epsilon}{\alpha E_S} \right)^{1/4}. \quad (23)$$

The estimate for the effective pair creation rate W_{cr} is less straightforward. Unlike for electrons, χ_γ can vary only at the scale $\sim \omega^{-1}$ as the photon traverses through the field. In a cascade, the emission and pair creation processes happen successively. To select the photons contributing the most, we should consider the interplay between two factors: (i) the pair creation is exponentially suppressed for $\chi_\gamma < 1$ but contributes at $\chi_\gamma \gtrsim 1$ [see Eq. (7)], and (ii) in the emission spectrum, softer photons with $\chi_\gamma \ll \chi_e$ dominate over the hardest ones with $\chi_\gamma \sim \chi_e$. Furthermore, one should note that γ_γ and χ_γ are related, since γ_e and χ_e of the emitting electron are mutually dependent in view of Eqs. (8)-(9).

In Fig. 3, we show examples of the emission spectra for two cases: for electrons with fixed γ_e and χ_e , and for electrons accelerated by a uniform rotating electric field so that γ_{em} and χ_{em} are consistent with Eqs. (11) and (12). We compare these curves to the probability rate of e^-e^+ pair creation by a photon in a rotating electric field. For this, we estimated $\chi_\gamma \sim \gamma_\gamma \epsilon / E_S$. The result suggests that at relatively low and high fields the dominating contribution to pair production is rendered by

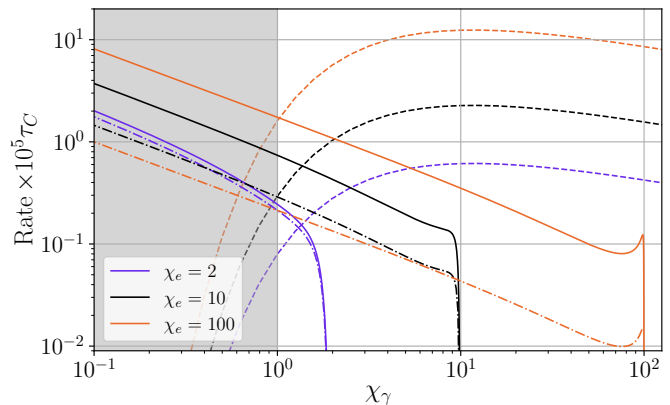


Figure 3. The spectrum of photons emitted by an electron $dW_{\text{cs}}(\gamma_e, \chi_e, \chi_\gamma)/d\chi_\gamma$ [Eq. (2)] and the total probability rate of e^-e^+ pair creation by a photon $W_{\text{BW}}(\gamma_\gamma, \chi_\gamma)$ [Eq. (5)] as a function of χ_γ . Solid lines stand for emission by an electron with $\gamma_e = 10^3$ and different values of χ_e . Dot-dashed lines correspond to emission by an electron accelerated by a uniform rotating electric field, so that $\gamma_e = \gamma_{\text{em}}$ and $\chi_e = \chi_{\text{em}}$ [see Eqs. (11), (12)]. Dashed lines show W_{BW} for a photon emitted in a uniform rotating field, so that γ_γ and χ_γ are consistent, $\gamma_\gamma \sim \chi_\gamma E_S / E_0$. The dashed and dot-dashed lines are plotted at the following values of $eE_0/(mc\omega)$: 2550 (purple), 9436 (black), and 51581 (orange), which gives $\chi_{\text{em}} = 2, 10$, and 100, respectively, for the field wavelength $\lambda = 2\pi c/\omega = 0.8\mu\text{m}$. In the grey-shaded area $\chi_\gamma < 1$, the pair creation probability is suppressed [see Eq. (7)].

different parts of the emission spectrum. Let us discuss these cases one by one.

At a relatively low field, such that χ_{em} barely exceeds 1, only the rightmost edge of the photon χ_γ distribution can contribute to the cascade (see the $\chi_e = 2$ line in Fig. 3). Then the pair creation rate can be estimated as

$$W_{\text{cr}}|_{\chi_{\text{em}} < \mathcal{X}} \sim W_{\text{BW}}(\gamma_\gamma = \gamma_{\text{em}}, \chi_\gamma = \chi_{\text{em}}), \quad (24)$$

where $1 \lesssim \mathcal{X} < 10$ sets the effective applicability range of the formula. We discuss it at the end of this subsection. Note that this is consistent with the (rough) cascade threshold condition proposed in Refs. [40, 42]. Namely, $\chi_{\text{em}} \gtrsim 1$ is the necessary requirement ensuring that the emitted photon can have $\chi_\gamma \sim 1$ and, hence, create a pair in a successive quantum event.

In a high field, electrons emit at $\chi_{\text{em}} \gg 1$, as we discussed in Section II D. All of the photons with $1 \lesssim \chi_\gamma \leq \chi_{\text{em}}$ can contribute to pair production, which represents a wide part of the distribution (see the orange lines in Fig. 3 corresponding to $\chi_{\text{em}} = 100$). Furthermore, the fraction of photons with $\chi_\gamma \sim 1$ significantly exceeds that of $\chi_\gamma \sim \chi_{\text{em}}$, which is not compensated for by the (slower) increase of the pair creation rate. Therefore, we evaluate the pair creation rate as

$$\begin{aligned} W_{\text{cr}}|_{\chi_{\text{em}} > \mathcal{X}} &\sim W_{\text{BW}}(\gamma_\gamma = \frac{E_S}{\epsilon}, \chi_\gamma = 1) \\ &= \frac{\epsilon}{E_S} W_{\text{BW}}(1, 1). \end{aligned} \quad (25)$$

Here, we estimated γ_γ from $\chi_\gamma \sim \overline{\gamma_\gamma \epsilon} / E_S := 1$. In the second line, we used that W_{BW} depends on $\gamma_\gamma \sim E_S / \epsilon$ only in the prefactor [see Eq. (3)].

Summarising, Γ depends on the (invariant) field strength ϵ entering the effective rates parametrically via $\gamma_{\text{em}}(\epsilon)$, $\chi_{\text{em}}(\epsilon)$. This dependence can be written for a general field by plugging the effective rates into Eq. (21):

$$\Gamma|_{\chi_{\text{em}} < \mathcal{X}}(\epsilon) \simeq \Gamma[W_{\text{CS}}(\gamma_{\text{em}}, \chi_{\text{em}}), W_{\text{BW}}(\gamma_{\text{em}}, \chi_{\text{em}})], \quad (26)$$

$$\Gamma|_{\chi_{\text{em}} > \mathcal{X}}(\epsilon) \simeq \Gamma[W_{\text{CS}}(\gamma_{\text{em}}, \chi_{\text{em}}), \frac{\epsilon}{E_S} W_{\text{BW}}(1, 1)]. \quad (27)$$

In these expressions, the rates W_{CS} and W_{BW} can be calculated numerically by using Eqs. (2)-(5), and ν can be extracted from simulations. We require that Eqs. (26) and (27) match at $\chi_{\text{em}} \sim \mathcal{X}$. This condition can be reexpressed in terms of the field strength in view of Eq. (15).

It is important to note that the crossover region for Eqs. (26)-(27) is finite, which is due to the following reason. The transition between the approximations for W_{cr} in Eqs. (24) and (25) is smeared, as for the electrons radiating with $1 \lesssim \chi_{\text{em}} < 10$ the relative decrease of the number of emitted photons with $\chi_\gamma \sim 1$ and $\chi_\gamma \sim \chi_{\text{em}}$ can be comparable [see the black curves in Fig. 3, corresponding to $\chi_{\text{em}} = 10$]. The photons with $\chi_\gamma \sim 1$ start to dominate in the spectrum at relatively high $\chi_{\text{em}} \gtrsim 10$. As a result, we can estimate the transition point \mathcal{X} by picking a value from the interval $1 \lesssim \mathcal{X} < 10$. Alternatively, it can be evaluated with higher precision by extracting Eqs. (26) and (27) from simulations and matching them.

C. Asymptotic behavior of Γ at low and high fields and the particle orbit dimensionality

Let us discuss the behavior of the growth rate in the limiting cases of a low and high field. We define a low/high field by the correspondence given in Eq. (16). In a weak field $\epsilon \ll \alpha E_S$, i.e. at $\chi_{\text{em}} \ll 1$, the emitted photons are soft, $\chi_\gamma \ll 1$, and the pair creation rate is exponentially small, see Eq. (7). At the same time, the probability for an electron to emit a soft photon stays finite. Assuming that $\nu \sim \omega / (2\pi)$, let us expand Eq. (26) at small $W_{\text{cr}} \ll \nu$, W_{rad} to the leading order:

$$\Gamma|_{\nu > 0}(\epsilon \ll \alpha E_S) \simeq \frac{W_{\text{BW}}(\gamma_{\text{em}}, \chi_{\text{em}})}{\nu} [2W_{\text{CS}}(\gamma_{\text{em}}, \chi_{\text{em}}) - \nu] \propto e^{-\frac{8}{3\chi_{\text{em}}}}. \quad (28)$$

If $\nu = 0$ (e.g. for a cascade developing in a uniform rotating electric field), the expansion results in a different scaling for the leading term (c.f. Eq. (8) in [45]):

$$\Gamma|_{\nu=0}(\epsilon \ll \alpha E_S) \simeq \sqrt{2W_{\text{CS}}(\gamma_{\text{em}}, \chi_{\text{em}})W_{\text{BW}}(\gamma_{\text{em}}, \chi_{\text{em}})} \propto e^{-\frac{4}{3\chi_{\text{em}}}}. \quad (29)$$

Hence, the particle migration leads to significant suppression of the cascade growth rate in the low field regime. It can be viewed as a topological effect: $\nu = 0$ corresponds

to an effective reduction of the particles' degrees of freedom as if they are confined in the strong field region (e.g. the center of the E -antinode of a standing field wave). This naturally amplifies the growth rate. The field dependence at low ϵ can be found explicitly by using the low- χ asymptotic of Eqs. (6), (7) and the low- ϵ expansion for $\gamma_{\text{em}}(\epsilon)$ and $\chi_{\text{em}}(\epsilon)$ [see also Eqs. (B4), (B5)]:

$$\Gamma(\epsilon \ll \alpha E_S) \approx \frac{\alpha}{\tau_C} \sqrt{\frac{\epsilon \omega_{\text{eff}} \tau_C}{\alpha E_S}} \times \begin{cases} 0.44 \left[3.40 \frac{\alpha}{\nu} \sqrt{\frac{\epsilon \omega_{\text{eff}} \tau_C}{\alpha E_S}} - 1 \right] e^{-1.92 \frac{\alpha E_S}{\epsilon}}, & \nu > 0, \\ 1.23 e^{-0.96 \frac{\alpha E_S}{\epsilon}}, & \nu = 0. \end{cases} \quad (30)$$

The asymptotic expressions with full numerical coefficients are relegated to Appendix B, see Eq. (B7).

At high field $\epsilon > \alpha E_S$, namely, in the regime when Eq. (27) for Γ applies, the probability rates increase as $W_{\text{rad}} \propto \epsilon^{1/4}$ and $W_{\text{cr}} \propto \epsilon$ [see Eqs. (23) and (25)]. The migration rate is bounded, $\nu \lesssim \omega$, hence, as the field grows, we can neglect it compared to W_{rad} and W_{cr} in Eq. (27):

$$\Gamma(\epsilon > \alpha E_S) \simeq \frac{\epsilon W_{\text{BW}}(1, 1)}{2E_S} \left[\sqrt{1 + \frac{8E_S W_{\text{CS}}(\gamma_{\text{em}}, \chi_{\text{em}})}{\epsilon W_{\text{BW}}(1, 1)}} - 1 \right]. \quad (31)$$

It means that at high ϵ , regardless of the global field structure in space, the cascade will be effectively confined to the strong field region, where the particle production is the most efficient. Put differently, only the local structure of the field, where the conditions are optimal, affects the cascade growth rate. This effect should be universal for the fields, in which avalanche cascades can onset and reach a steady state.

By substituting in Eq. (31) the asymptotic expressions for the rates given by Eqs. (23), (25), we obtain the explicit field dependence of the growth rate in the high-field regime:

$$\Gamma(\epsilon > \alpha E_S) \simeq \frac{c_1 \epsilon}{\tau_C E_S} \left[\sqrt{1 + c_2 \sqrt{\omega_{\text{eff}} \tau_C} \left(\frac{\alpha E_S}{\epsilon} \right)^{3/4}} - 1 \right], \quad (32)$$

where the numerical coefficients $c_1 \approx 0.52 \times 10^{-4}$, $c_2 \approx 1.1 \times 10^5$ are defined in Eqs. (B8), (B9) in Appendix B. Here, we note that their magnitude is determined by $\tau_C W_{\text{BW}}(1, 1) \approx 1.03 \times 10^{-4}$.

Since $W_{\text{rad}} \propto \epsilon^{1/4}$ grows slower with ϵ as compared to $W_{\text{cr}} \propto \epsilon$, at asymptotically high fields the latter will become so large that $8W_{\text{rad}}/W_{\text{cr}} \ll 1$, and Eqs. (31), (32) simplify even further:

$$\Gamma(\epsilon \gg \alpha E_S) \simeq 2W_{\text{CS}}(\gamma_{\text{em}}, \chi_{\text{em}}) \propto \alpha \sqrt{\frac{\omega_{\text{eff}}}{\tau_C}} \left(\frac{\epsilon}{\alpha E_S} \right)^{1/4}. \quad (33)$$

For the rotating electric field configuration [see Eq. (10)] this corresponds to the scaling proposed by Fedotov et al. [40] (recall that for this case $\epsilon = E_0$, $\omega_{\text{eff}} = \omega/2$):

$$\Gamma_{\text{rot.-}E}(E_0 \gg \alpha E_S) \sim \alpha \sqrt{\frac{\omega}{\tau_C}} \left(\frac{E_0}{\alpha E_S} \right)^{1/4}. \quad (34)$$

The condition $W_{\text{cr}} > 8W_{\text{rad}}$ gives the estimate for the field at which this asymptotic starts to set in. By plugging in the explicit high-field expressions (23) and (25) for the rates, we arrive at the condition $E_0 > 3.35 \times 10^6 \alpha (\omega \tau_C)^{2/3}$. For the optical wavelength $\lambda = 0.8 \mu\text{m}$, this corresponds to the field strength $E_0 > 5E_S$, which is beyond the applicability range of the semiclassical approach. Notably, the scaling (34) was never confirmed by simulations in past works [43, 45, 46], as this range of field strengths was not studied.

IV. CASCADES IN A CP STANDING WAVE AT LOW AND MODERATE FIELDS ($\chi_{\text{em}} < \mathcal{X}$)

We apply our model to study the development of e^- -seeded cascades in a CP EM standing wave and test the model against simulations. This field configuration can be formed by two counterstreaming CP EM plane waves (with the opposite sign of polarization) so that the total electric and magnetic field components read:

$$\mathbf{E} = E_0 [\cos(kz) \sin(\omega t) \hat{\mathbf{x}} + \cos(kz) \cos(\omega t) \hat{\mathbf{y}}], \quad (35)$$

$$\mathbf{B} = -\frac{E_0}{c} [\sin(kz) \sin(\omega t) \hat{\mathbf{x}} + \sin(kz) \cos(\omega t) \hat{\mathbf{y}}], \quad (36)$$

where $k = \omega/c$, z is the axis of propagation, and E_0 is the electric field amplitude. The distribution of the electric and magnetic field strength along the longitudinal axis is illustrated in Fig. 4. At the electric antinode center, the magnetic field vanishes, and the electric field corresponds to the rotating E -field given in Eq. (10). The values of ϵ and ω_{eff} depend on the longitudinal coordinate. At the E -antinode centre ($z = 0$ in Fig. 4), $\epsilon = E_0$ and $\omega_{\text{eff}} = \omega/2$ as in a rotating E -field, and the combination $\epsilon^2 \omega_{\text{eff}}$ is maximal. In the B -antinodes (e.g. $\lambda/8 < z < 3\lambda/8$), $\epsilon^2 \omega_{\text{eff}}$ vanishes, hence, electrons do not gain χ_e [see Eq. (9)], and the cascade cannot be sustained in these regions.

A. PIC simulations

We study the electron-seeded cascade development numerically in both the standing wave and the uniform rotating E -field configurations. The calculations are performed with the PIC-QED code SMILEI [91] in 1D3V geometry. For further comparison, we also run full 3D PIC-QED simulations in a realistic setup where the standing wave is formed by two counterpropagating Gaussian beams.

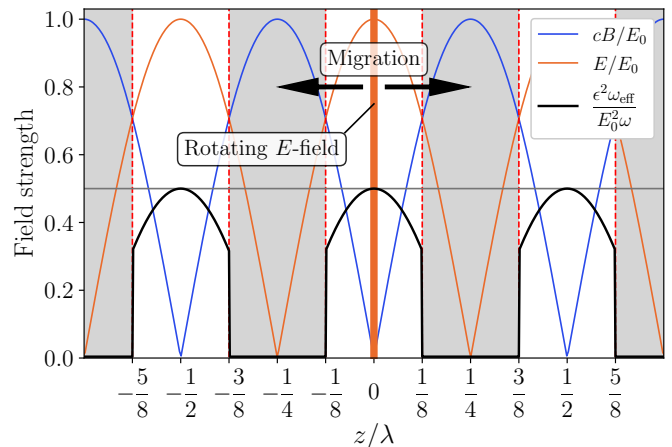


Figure 4. The longitudinal structure of the electric E and magnetic B field amplitude of a CP standing wave [see Eqs. (35) and (36)]. At the E -antinode center (shown by the thick vertical line), the magnetic field vanishes and the electric field rotates in the transverse plane [described by Eq. (10)]. The black line represents the longitudinal coordinate dependence of the $\epsilon^2 \omega_{\text{eff}}$ value entering the expression for $\chi_e(t)$, see Eq. (9). In the grey-shaded areas delimited by red dashed lines, it is zero, therefore, $\chi_e(t)$ for e^\pm is not restored in between the emission events. Electrons and positrons migrate from the E -antinode to the grey-shaded areas at characteristic time $t \sim 2\pi/\omega$ (shown by arrows), as the B -antinodes are the spiraling attractors for charged particles [79, 80, 105–107].

The numerical setup is detailed in Appendix E, though, let us mention some important points. The seed electrons are injected at time $t = 0$ into the electric antinodes in the simulations with a standing wave, and distributed homogeneously in the simulation box for the rotating E -field configuration. We fix the field frequency so that it corresponds to the optical laser wavelength $\lambda = 0.8 \mu\text{m}$, and we study the development of avalanches with time at varying E_0 . We keep the particle density low during the whole simulation so that collective effects are insignificant.

In the discussion of our model for Γ [given in Eq. (21)] in the standing wave configuration, we use the migration rate field dependence $\nu(E_0)$ calculated as follows. We inject the initial electrons in the vicinity of the E -antinode center $z = 0$, where $\epsilon^2 \omega_{\text{eff}}$ is maximal and the cascade onset is optimal (see Fig. 4). As the cascade develops, particles migrate to the B -antinodes, which are the spiraling attractors for charges [79, 80, 105–107]. When an electron reaches a spatial region at $|z| > \lambda/8$ where $\epsilon^2 \omega_{\text{eff}} = 0$, we consider this e^- is dropped out of the cascade. We define ν as the average inverse time at which initial particles propagate at distance $\lambda/8$ from the origin and extract it from simulations (for more details, refer to Appendix E).

In each simulation, we ensure that the cascade reaches a steady state so that it exhibits exponential growth of the particle number. We extract the growth rate by using the two following methods. First, we directly calcu-

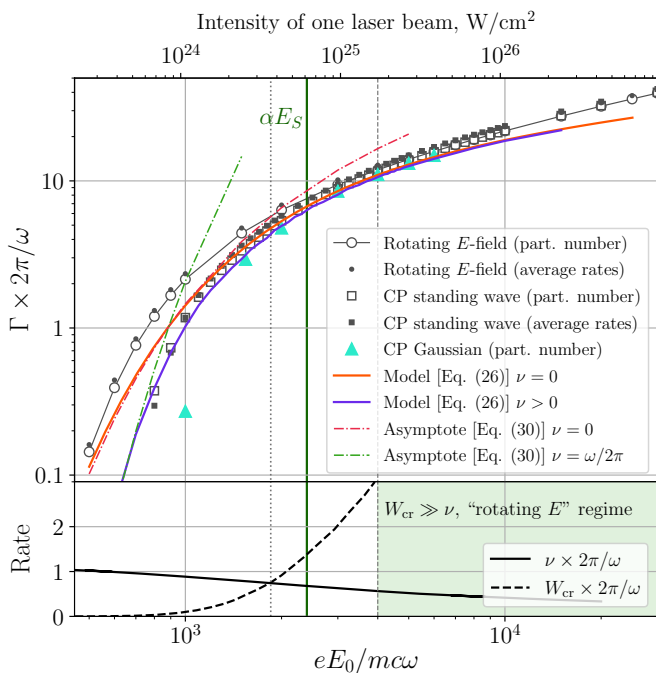


Figure 5. Top panel: the growth rate of an avalanche-type cascade as a function of the field amplitude E_0 in different field configurations. We plot the results of simulation obtained with SMILEI PIC for: CP standing wave [see Eqs. (35), (36)] (1D3V simulation), a uniform rotating electric field [see Eq. (10)] (1D3V simulation), CP standing wave formed by two Gaussian beams (full 3D simulation). Empty circles and squares correspond to Γ extracted directly from the particle numbers [see Appendix E]. Small filled circles and squares correspond to Eq. (21) with $W_{\text{rad,cr}} = \langle W_{\text{CS,BW}}(\gamma, \chi) \rangle$ averaged over the particle distributions reached at the end of each simulation. We compare the numerical data to our model given in Eq. (26) both with and without accounting for the migration effect and to the corresponding asymptotic expressions from Eq. (30). Bottom panel: migration rate ν in a CP standing wave extracted from 1D3V PIC simulations, and estimated pair production rate [see Eq. (24)]. For reference purposes, we put a secondary horizontal axis at the top in the intensity units of a single laser beam of the amplitude $E_0/2$, implying that the standing wave is formed by two of such laser beams [c.f. Eqs. (35)-(36)]. For all the curves, the field wavelength is set to $\lambda = 0.8\mu\text{m}$.

late Γ by fitting the e^-e^+ pair number time dependence $N_p(t)$ with the exponential function $e^{\Gamma t}$ (the full procedure is described in Appendix E). Second, as discussed in Section III A, the exact growth rate given in Eq. (21) with the effective rates $W_{\text{rad,cr}}$ evaluated as prescribed by Eq. (20). We extract the steady-state distribution functions $f_{e,\gamma}(\gamma_{e,\gamma}, \chi_{e,\gamma})$ from the numerical data and calculate the corresponding values $\langle W_{\text{CS,BW}}(\gamma, \chi) \rangle$ [see also Eqs. (C21)-(C22) in Appendix C]. Then we plug this result and the migration rate $\nu(E_0)$ (calculated as explained above) in Eq. (21) to obtain Γ .

The simulation results and the comparison with the theoretical models for the described field configurations

are presented in Fig. 5. We plot the extracted cascade growth rate for E_0 varied from a (relatively) low value, when the cascade multiplicity is exponentially small, to a strong field with high particle yield. The migration rate field dependence $\nu(E_0)$ is also shown in the bottom panel.

We confirm the full consistency of the numerical data for Γ obtained directly from $N_p(t)$ (shown in Fig. 5 with empty circles and squares for the rotating E -field and standing wave configurations, respectively) with formulas (20)-(21) (depicted with small filled round and square markers). This result substantiates our argumentation from Section III A and Appendix C that the master equations and their solution, given in Eqs. (18)-(21), are exact. It also validates our method of accounting for particle migration by using the rate $\nu(E_0)$. Let us note that a small discrepancy between the two methods for Γ extraction is explained by the unideal determination of the steady state due to the limitations of our numerical approach in the low field regime.

B. Validation of the analytical model

We plot our model for Γ given in Eq. (26) and test it against simulations (see solid lines in Fig. 5). Recall that in this case, we calculate the rates as $W_{\text{rad,cr}} = W_{\text{CS,BW}}(\gamma_{\text{em}}, \chi_{\text{em}})$, where γ_{em} and χ_{em} are evaluated by combining Eqs. (11) and numerically integrated Eq. (12).⁵ Apart from the high field region (which we discuss in the next Section), the model shows excellent agreement with the simulation results for both configurations: the standing wave (compare the purple curve and empty squares in Fig. 5) and rotating E -field (compare the orange curve and empty circles *ibid*). In the former, we take into account the particle migration by using the numerical data for $\nu(E_0)$. However, we note here that by using a simple estimate $\nu = 1/T = \omega/(2\pi)$ we obtain a very close result (refer to the purple line).

Among the cases we studied, the uniform rotating E -field provides the highest pair yield. As compared to it, Γ for a cascade in a standing wave is substantially smaller at low E_0 , which is due to e^-e^+ migration. The exponential decay of the rate for the asymptotically low fields is faster for the standing wave configuration, which correlates with the prediction by our model, see Eqs. (28)-(30) (also plotted in Fig. 5 with thin dot-dashed lines). The effect of migration is even stronger in the field of two Gaussian beams, as particles can also escape in the direction transverse to the optical axis.

At low E_0 , the growth rate can be small as compared to the inverse field period, $\Gamma \times 2\pi/\omega \ll 1$, meaning that

⁵ We assume that the main contribution to the cascade growth rate comes from the particles the E -antinode center of a standing wave, therefore, when calculating γ_{em} and χ_{em} , we set $\epsilon = E_0$ and $\omega_{\text{eff}} = \omega/2$ as in a rotating E -field.

the setting time for the steady state can be also much larger than $2\pi/\omega$. In this case, the growth rate can be limited not only by migration but also by the finite pulse duration. In this case, our model can be used for an estimate of the average particle yield during the interaction.

With growing E_0 , the simulation results and the model predictions for Γ in the standing wave configuration approach the optimal case of a rotating E -field. Moreover, the growth rate of a cascade in the field of Gaussian beams also shows the same behavior. At the same time, the migration rate decreases and becomes small compared to the effective pair creation rate by photons, as shown in the bottom panel of Fig. 5. In effect, the cascade develops at the E -antinode center. The model of a uniform rotating E -field becomes *universal* for all CP standing wave-like configurations. Notably, the orbits of individual particles become 2-dimensional. This illustrates the discussion in Section III C.

The transition to the reduced dynamics takes place at $E_0 \sim \alpha E_S$, therefore, at higher fields it is enough to consider only the rotating electric field model for calculating the particle growth rate. Moreover, as the field increases the growth rate given by Eq. (26), as expected, deviates from the numerical results (see Fig. 5) and has to be replaced by Eq. (27). This will be addressed in the following Section.

V. CASCADES IN HIGH CP FIELDS ($\chi_{\text{em}} > \mathcal{X}$)

A. Modelling the cascade growth rate in the full range of field strength

Let us discuss the growth rate of avalanches at very high fields focusing specifically on the uniform rotating electric field configuration.⁶ We extend our simulations with SMILEI to higher E_0 using the setup presented in Section IV A and Appendix E. In addition, we perform independent 3D simulations with a semiclassical Monte-Carlo code [44]. In the latter case, the external field is described by Eq. (10), and the results are averaged over $\sim 10^2$ runs, where each run is initialized with one seed electron at rest. The results are presented in Fig. 6. The data obtained with both codes matches with high precision.

In Fig. 6, we plot the previously discussed Eq. (26) and present the growth rate model developed for high fields, namely, Eq. (27). The latter expression matches the data points in the high field region, which is not covered by Eq. (26). The curves overlap in an extended interval of E_0 at $E_0 \gtrsim \alpha E_S$. The full model is rendered by linking both expressions (highlighted with green in Fig. 6). Let us point out here, that at the overlap χ_{em} varies from ≈ 3 to 10 (also shown in Fig. 2). This corresponds to

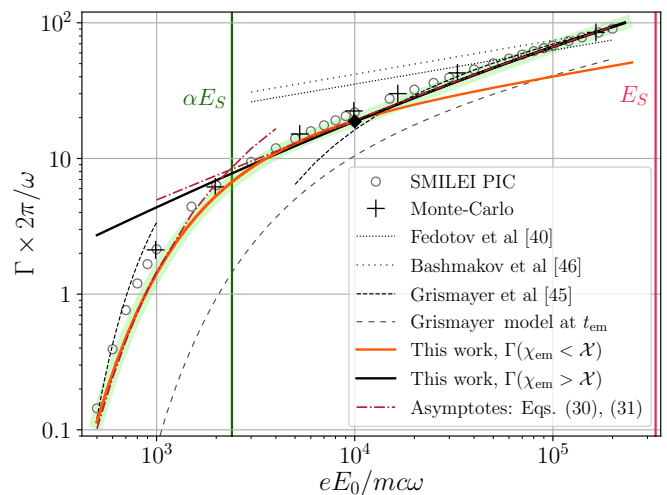


Figure 6. Cascade growth rate dependence on E_0 in a uniform rotating electric field obtained in simulations (circles and cross markers). The solid curves represent the model proposed in this work. The full model (highlighted in green) is obtained by switching from Eq. (26) [in orange] to Eq. (27) [in black] when they overlap (marked by the black diamond). Note that we partially duplicate the data from Fig. 5, keeping the same notation. Here, $\lambda = 0.8\mu\text{m}$.

the matching condition for Eqs. (26) and (27), which we considered in Section III B.

We also plot in Fig. 6 the asymptotic expressions for Γ at low and high fields, given in Eqs. (30) and (32), respectively. The latter fits the black curve at $E_0 > \alpha E_S$ with high precision, namely, almost in the whole region of Eq. (27) applicability. The two asymptotic expressions cross at $E_0 \sim \alpha E_S$. As a result, when combined, they provide a simple yet robust explicit formula for the field dependence of the avalanche growth rate.

Recall that our model in (27) for high fields $E_0 > \alpha E_S$ incorporates the pair creation rate by photons at $\chi_\gamma \sim 1$, as we expect them to dominate in the emission spectrum. We confirm this assertion with simulations. We extract the steady-state photon distribution function $f_\gamma(\gamma_\gamma, \chi_\gamma)$, which is normalised by the condition $\int d\gamma_\gamma d\chi_\gamma f_\gamma(\gamma_\gamma, \chi_\gamma) = 1$. We then weight it with the rate W_{BW} to identify the photons that contribute to the process of pair creation. The weighted distribution in χ_γ is defined by

$$[W_{\text{BW}} * f_\gamma](\chi_\gamma) = \int d\gamma_\gamma W_{\text{BW}}(\gamma_\gamma, \chi_\gamma) f_\gamma(\gamma_\gamma, \chi_\gamma). \quad (37)$$

We plot this expression for different E_0 in Fig. 7. As we anticipated in our model, the weighted distribution peaks at $\chi_\gamma \approx 2$ for $E_0 > \alpha E_S$. At the same time, χ_{em} of emitting electrons increases with the field (see also Fig. 2). In the example of a lower field, $E_0 \approx 0.4\alpha E_S$, the curve maximum is shifted to the left as compared to the others, and the corresponding χ_{em} is shifted leftwards even further. Thus only the exponential tail of the photon distribution can contribute to pair creation, so the avalanche

⁶ Throughout Section V, we assume that $\nu = 0$.

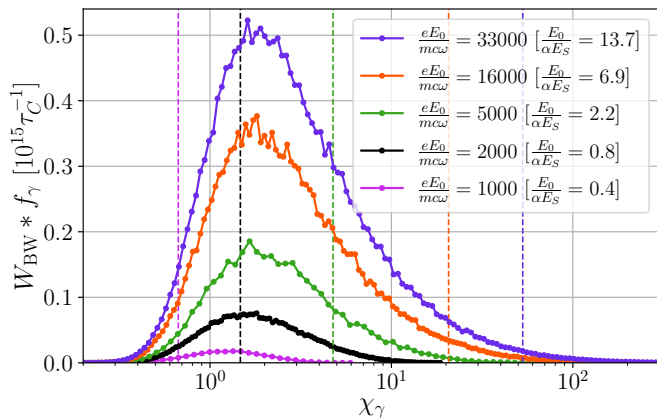


Figure 7. Distribution of photons $f_\gamma(\chi_\gamma)$ in a cascade in the steady state weighted with the probability rate of pair creation W_{BW} for different values of field strength [for the definition, see Eq. (37)]. The data is extracted from Monte-Carlo simulations. The vertical dashed lines represent the characteristic value of χ_{em} for electrons at the emission event [as defined in Eq. (15)]. For each of the dashed lines, χ_{em} is calculated at E_0 respective to a $W_{\text{cr}}f_\gamma$ graph of the same color.

development is suppressed (see the corresponding growth rate in Fig. 6). At $E_0 \approx 0.8\alpha E_S$, the value of $\chi_{\text{em}} \approx 1.4$ is close to the peak of the corresponding weighted distribution. Hence, both the emission and pair creation rates are far from their asymptotic given in Eqs. (6), (7), and we can associate the region $E_0 \sim \alpha E_S$ to the transition between the low and high field regimes.

B. Comparison to the growth rate models proposed in past works

Let us discuss how our model compares to the results of previous works. The available growth rate models for the uniform rotating electric field configuration are summarised in Table I. The scaling $\Gamma \propto E_0^{1/4}$ at $E_0 \gg \alpha E_S$ was first obtained by Fedotov et al [40, 43]. The coefficient for this scaling can be refined by using the result of Bashmakov et al [46], where it was initially proposed to use the analog of Eq. (21), which, however, does not account for the migration effect and implies using $W_{\text{rad,cr}}$ estimated in the spirit of Refs. [40, 43]. Both results are plotted in Fig. 6. Although they give the right order of magnitude estimate at high E_0 , the $E_0^{1/4}$ scaling sets in only beyond E_S (for a laser field of the optical frequency), as we mentioned at the end of Sec. III C. In contrast to that, our formula (32) provides reliable high-field scaling at $E_0 > \alpha E_S$.

In our notations, the scaling of Fedotov et al [40, 43] is based on the assumption that $\chi_\gamma \sim \chi_{\text{em}}$, therefore, it does not account for the emission spectrum shape. For instance, the probability rate of two successive events of photon emission and pair creation by this photon (in the steady state) would be proportional to $P_{e^- \rightarrow e^- e^+} \propto$

$W_{\text{rad}}W_{\text{cr}} \sim W_{\text{rad}}^2$. Grismayer et al [45, 63] proposed a phenomenological model improving on that front. Put concisely, it is achieved by expressing this probability as

$$P_{e^- \rightarrow e^- e^+} \propto \int_0^{\bar{\chi}_e} d\chi' \frac{dW_{\text{cs}}(\bar{\gamma}_e, \bar{\chi}_e, \chi')}{d\chi'} W_{\text{BW}}(\varepsilon', \chi') \quad (38)$$

where $\bar{\gamma}_e$, $\bar{\chi}_e$ are the characteristic values at the moment of emission, which depend on the field and are kept general in this step. We re-derive the formula for the growth rate proposed by Grismayer et al using the kinetic approach, see Appendix D, where we also clarify the approximations needed to get the result. It results in transcendental equation (D7) for Γ , which can be solved numerically once the expressions for $\bar{\gamma}_e$, $\bar{\chi}_e$ are known. In Ref. [45], this calculation was carried out at asymptotically low and high fields.

Recall that in Section III A we argue that our model based on Eqs. (18)-(21) incorporates the emission spectra without additional approximations. Let us compare our results against the model of Grismayer et al.

For a low field, Grismayer et al propose setting $\bar{\gamma}_e \propto E_0$, $\bar{\chi}_e \propto E_0^2$ (see Table I) extracted from classical dynamics of an electron averaged over the field cycle. The thin dashed line in Fig. 6 illustrates the resulting growth rate. Notably, the asymptotic decays as $\propto \exp[-8/(3\bar{\chi}_e)]$, which is steeper than in our model Eq. (29) [see also Table I]. Though, the numerical data falls in between the two asymptotes.

In the high field regime, Grismayer et al use the E_0 -scaling for $\bar{\gamma}_e$, $\bar{\chi}_e$ derived by Fedotov et al from the short time dynamics [we write the corresponding expressions valid for a general field in Eqs. (B4), (B5)] with one additional modification, such that $\bar{\chi}_e$ is defined as $\bar{\chi}_e := A[E_0/(\alpha E_S)]^{3/2}$, where $A := 1.24$ is a free parameter used to fit the numerical data. The fit allows matching the data by the asymptote at very high E_0 , as shown in Fig. 6. The results of Grismayer et al are close to our predictions. The advantage of our model is that it does not require fitting parameters.

The study in Ref. [45] did not cover the intermediate regime due to the lack of the corresponding expressions for $\bar{\gamma}_e$, $\bar{\chi}_e$. As we propose them in Section II C, namely, γ_{em} and χ_{em} , we tested the model of Grismayer et al in the full range. The result is shown in Fig. 6 (the sparse-dashed line).⁷ Unfortunately, the result significantly underestimates the particle growth rate, which is, presumably, because of the overall pair production rate undercount. The radiation and pair creation events are coupled in Eq. (38): χ' of the emitted photon also enters W_{BW} , namely, the photon supposedly decays into a pair shortly after the emission event. In our model, these processes are decoupled, as rates W_{rad} , W_{cr} are calculated independently. The possible variation of $\chi_{e,\gamma}$ in between

⁷ We assigned $\bar{\gamma}_e := \gamma_{\text{em}}$, $\bar{\chi}_e := \chi_{\text{em}}$ without the fitting parameter used in Ref. [45].

Table I. Summary of the particle growth rate models in avalanche-type QED cascades developing in a uniform rotating electric field. The table collects the results of Refs. [40, 43, 45, 46, 63], and this paper.

Reference	χ_e	γ_e	χ_γ	W_{rad}	W_{cr}	Γ
[40] ^{Fedotov} , [43] ^{Elkina}	$\mu^{3/2}$, ^a	$\frac{\mu^{3/4}}{\sqrt{\omega^*}}$	$\sim \chi_e \gg 1$	$\sim \frac{\alpha \chi_e^{2/3}}{\tau_C \gamma_e}$	W_{rad}	$\sim \frac{\alpha \mu^{1/4}}{\tau_C \sqrt{\omega^*}}$
[46] ^{Bashmakov}	$0.57 \mu^{3/2}$	$\approx \frac{\mu^{3/4}}{\sqrt{\omega^*}}$	$\sim \chi_e \gg 1$	$W_{\text{CS}}(\chi_e \gg 1)$ ^b	$W_{\text{BW}}(\chi_\gamma \gg 1)$	Eq. (21) at $\nu = 0$
[45] ^{Grismayer} low E_0	$\frac{(\alpha \mu)^2}{\omega^*}$	$\frac{4\alpha \mu}{\pi \omega^*}$	$0 < \chi_\gamma \leq \chi_e$ ^c	–	$W_{\text{BW}}(\chi_\gamma \ll 1)$	$C_1 \frac{\alpha^2 \mu}{\tau_C} e^{-\frac{8\omega^*}{3\alpha^2 \mu^2}}$, ^d
[45] ^{Grismayer} high E_0	$1.24 \mu^{3/2}$	$\frac{\mu^{3/4}}{\sqrt{\omega^*}}$	$0 < \chi_\gamma \leq \chi_e$ ^c	$W_{\text{CS}}(\chi_e \gg 1)$	$W_{\text{BW}}(\chi_\gamma)$	Root of Eq. (D7)
This work $E_0 < \alpha E_S$	$C_2 \mu$	$\sqrt{2C_2} \sqrt{\frac{\mu}{\omega^*}}$	$\sim \chi_{\text{em}}$	$W_{\text{CS}}(\chi_{\text{em}} \ll 1)$	$W_{\text{BW}}(\chi_{\text{em}} \ll 1)$	$C_3 \frac{\alpha \sqrt{\mu \omega^*}}{\tau_C} e^{-\frac{5}{3\sqrt{3}\mu}}$
This work $E_0 > \alpha E_S$	$C_4 \mu^{3/2}$	$\sqrt{2C_4} \frac{\mu^{3/4}}{\sqrt{\omega^*}}$	~ 1	$W_{\text{CS}}(\chi_{\text{em}} \gg 1)$	$W_{\text{BW}}(1)$	$\frac{c_1 \alpha \mu}{\tau_C} \left[\sqrt{1 + c_2 \sqrt{\omega^*} \mu^{3/4}} - 1 \right]$

^a For brevity, we define the dimensionless quantities $\mu = E_0/(\alpha E_S)$, $\omega^* = \omega \tau_C = \hbar \omega / (mc^2)$.

^b To keep the table concise, we omit $\gamma_{e,\gamma}$ in the argument of $W_{\text{CS,BW}}$ [see Eqs. (4), (5)]; for the asymptotic expressions see Eqs. (6)-(7).

^c The χ_γ distribution is given by $dW_{\text{CS}}/d\chi_\gamma$, see Eq. (2).

^d The numerical constants: $C_1 = \pi^{3/2}/(20 \cdot 6^{1/4}) \approx 0.18$, $C_2 = 4\sqrt{3}/5 \approx 1.39$, $C_3 = 3^{5/6} \sqrt{5} \Gamma^2(2/3)/(\sqrt{14}\pi) \approx 0.87$, $C_4 = 9(2/[7\Gamma(2/3)])^{3/2} \approx 0.87$, for $c_{1,2}$ see Eqs. (B8), (B9).

the quantum processes is taken into account implicitly. As a result, we were able to reproduce the numerical data with Eqs. (26) and (27) in the full range of E_0 without using free parameters (apart from the model matching point choice).

VI. FORMATION OF ELECTRON-POSITRON PLASMA IN AVALANCHE-TYPE CASCADES

We apply our model to estimate the threshold for electron-positron plasma formation in a cascade in terms

of field parameters. Let us assume that a cascade is triggered in a uniform rotating electric field by electrons with initial density n_0 . At time t the particle density will reach $n(t) = n_0 \exp(\Gamma t)$. For a field of an optical frequency, Γ is well estimated by the asymptotic expressions (30) and (32) matched at their crossing point. By using them, we can calculate the time required to reach density n :

$$t \simeq T \ln \left(\frac{n}{n_0} \right) \times \begin{cases} 6.74 \cdot 10^{-2} \sqrt{\frac{1000}{a_0}} \exp \left[2.89 \left(\frac{1000}{a_0} \right) \left(\frac{\lambda}{1 \mu\text{m}} \right) \right], & a_0 < 3000 \left(\frac{\lambda}{1 \mu\text{m}} \right), \\ \frac{3.31 \cdot 10^{-2} \left(\frac{1000}{a_0} \right)}{\sqrt{1 + 278.5 \sqrt[4]{\left(\frac{1000}{a_0} \right)^3 \left(\frac{\lambda}{1 \mu\text{m}} \right)} - 1}}, & a_0 > 3000 \left(\frac{\lambda}{1 \mu\text{m}} \right) \end{cases} \quad (39)$$

where we used the notation $a_0 = eE_0/(mc\omega)$.

Eq. (39) allows to identify two characteristic times. First, the time t_c at which the produced particles reach the critical electron plasma density, $n(t_c) = n_c = \varepsilon_0 m \omega^2 / e^2$, and second, t_{scr} corresponding to the time moment when the plasma starts to screen the external field, $n(t_{\text{scr}}) = a_0 n_c$. The field dependence for these quantities is plotted in Fig. 8. The time needed to reach an e^-e^+

plasma state is exponentially large at low field, but for $a_0 \gtrsim 10^3$ it can be reached in several or even one field cycle depending on the initial density n_0 . Backreaction from the produced plasma should become noticeable after one field cycle at $a_0 \gtrsim 5 \cdot 10^3$ (for optical lasers) if $n_0 \gtrsim 10^{-3} n_c$. Note that the corresponding field strength is $E_0 \gtrsim \alpha E_S$.

We calculated the characteristic screening time t_{scr} in

the rotating E -field configuration through PIC simulations with SMILEI. The numerical setup is the same as for the previous simulations in Sections IV, V and is detailed in Appendix E. Here, we extended the time of each simulation so that the produced plasma could generate a noticeable field.

To identify the significance of the plasma-generated field, we used the following convenient technical feature of SMILEI. We generated two sets of simulations under the same input parameters: with so-called test and real particles. The formers do not generate self-fields, therefore, a corresponding simulation is equivalent to a semiclassical Monte-Carlo computation.⁸ The particle growth rate in such simulations remains constant in time once the steady state is reached. In contrast, when the density of real particles becomes high, the external field is screened, and the cascade growth rate can be reduced. The magnitude of screening can be guessed from the relative difference in the particle numbers obtained in the two simulations, $\delta N = (N_{\text{test}} - N_{\text{real}})/N_{\text{test}}$. As δN increases with time, t_{scr} can be associated with the time moment when δN reaches a prescribed threshold value.

The results of PIC simulations are presented in Fig. 8. Each of the (square) points corresponds to a time moment t_{scr} such that $\delta N(t_{\text{scr}}) = 0.15$. The inset illustrates our method for extracting t_{scr} for one of the plotted points. Note that variation of the threshold value for δN does not lead to a significant change in the results. The simulation results show good correspondence to the prediction of our model. Let us remark that we did not account for the migration. For t_{scr} at lower fields, that require several field revolutions to generate dense plasma, migration will lead to even longer times. However, at $E_0 \gtrsim \alpha E_S$, t_{scr} becomes comparable to the field period, and at the same time the effect of migration becomes negligible (as we discussed in previous sections).

VII. SUMMARY AND DISCUSSION

In the present work, we considered electron-seeded avalanche-type (or self-sustained) QED cascades developing in the field of a strong circularly polarized standing EM wave. Cascades in this configuration were investigated in past works including [38–40, 43, 45–47, 62, 63] mainly relying on numerical simulations. Our major goal was identifying the analytical time- and field-dependence of the particle numbers produced in such a cascade.

For optimal particle yield in such a configuration, it is useful to inject seed particles into the electric antinodes, where the acceleration of charged particles is maximal. However, charges can migrate to the magnetic antinodes at rate ν reducing the cascade efficiency. Our work highlights that this effect is important below a certain field

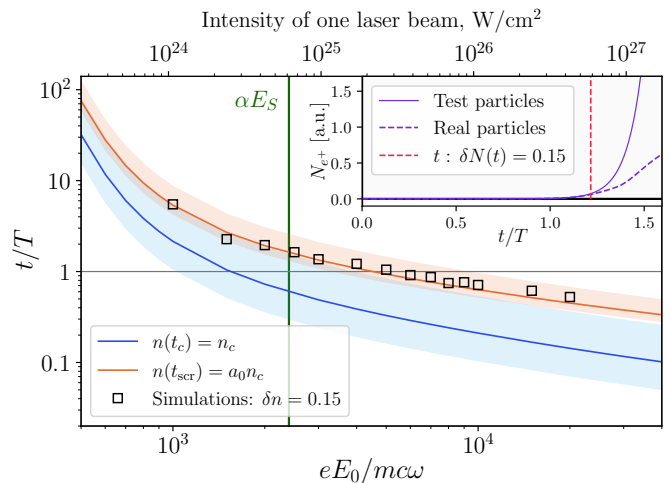


Figure 8. The field strength dependence of the time required to reach the electron critical plasma density n_c (blue) and the relativistically opaque regime $a_0 n_c$ (orange) in a cascade in a uniform rotating electric field. The time depends on the initial electron density n_0 , which is depicted as color bands: the lower bound corresponds to $n_0 = 10^{-5} n_c$, and the upper to $n_0 = 10^{-1} n_c$. Solid lines correspond to $n_0 = 10^{-3} n_c$. The inset shows two sample simulations in SMILEI: with real and test particles. Squares in the main plot correspond to a time point when $\delta N = (N_{\text{test}} - N_{\text{real}})/N_{\text{test}}$ reaches the value of 0.15. For reference purposes, we put a secondary horizontal axis at the top in the intensity units of a single laser beam of the amplitude $E_0/2$. The wavelength is set to $\lambda = 0.8 \mu\text{m}$.

threshold since it raises the field strength necessary to trigger a cascade. Understanding the impact of migration is critical to make the optimal choice of field configuration in upcoming experiments at ultra-high-intensity laser facilities, in particular because the first tests will take place near the cascade onset threshold.

At the onset stage, the cascade evolution is highly non-stationary. Nonetheless, the system can rapidly relax to the so-called steady state, in which the effective rates of photon emission W_{rad} , pair creation W_{cr} , and migration ν are constant and depend only on the field parameters. The steady-state master equations for the particle number can be cast in a simple form: Eqs. (18)-(19). We derive these equations by using a rigorous kinetic approach (detailed in Appendix C) relying only on the LCFA. We demonstrated that the values for $W_{\text{rad,cr}}$, that enter the master Eqs. (18)-(19), are obtained by averaging the total emission and pair creation rates given in Eqs. (4) and (5) over the particle distributions. The solution to the steady-state equations shows an exponential growth $N_{e^{\pm},\gamma} \sim e^{\Gamma t}$, where the growth rate Γ is given by Eq. (21).

An explicit calculation of Γ would provide the desired $N_{e^{\pm},\gamma}$ field dependence, however, the analytic expressions for the distribution functions and, hence, for the average rates $W_{\text{rad,cr}}$ and ν are unknown. Therefore, we developed a refined model for the rates. Simple relations for the short-time semiclassical electron dynamics in the cas-

⁸ Technical details can be found in the SMILEI code manual <https://smileipic.github.io/Smilei/>.

Table II. Single CP laser beam intensity [W/cm²] required to produce (on average) one e^-e^+ pair per seed electron during one field period in an avalanche-type cascade triggered in the CP field of two such counterpropagating lasers. Here, we assume that the laser wavelength is $\lambda = 0.8\mu\text{m}$.

	Rotating E	CP standing wave	Gaussian beams
Model	6.5×10^{23}	8.8×10^{23}	—
Simulation	5×10^{23}	8.5×10^{23}	1.1×10^{24}

cade allow defining the characteristic values of the key parameters $\chi_{e,\gamma}$, at which the photon emission or pair creation events are likely to happen (see Section II C).

As a result, we were able to calculate the effective rates as given in Eqs. (22), (24), and (25). These expressions allowed us to identify the growth rates Eqs. (26), (27) and their asymptotic forms, (30) and (32). Let us emphasize, that Eqs. (26), (27) for Γ are valid for a wide range of field models and parameters, with the major requirement that a cascade can onset and then reach the steady state.

To test the model, we performed extensive numerical simulations with the PIC-QED code SMILEI [91] and a Monte Carlo code [42, 44]. We considered three field configurations: the electric antinode of an infinite standing CP wave, the uniform rotating electric field (migration is absent in this case), and two counterpropagating tightly focused CP Gaussian beams representing a realistic laser field (the setup parameters are detailed in Appendix E). First, we demonstrated that the steady state equations (18)-(19) describe the evolution of the particle numbers precisely when the effective rates are calculated as averages over the particle distributions. Second, we confirmed that our model for the growth rate [Eqs. (26)-(27)] is in excellent agreement with the numerical data.

As we expected, at lower fields the migration of particles significantly suppresses the cascade growth rate as compared to the best-case scenario of a uniform rotating E -field. Notably, this happens in the parameter range of the upcoming experiments at the new generation of multi-petawatt laser facilities. We provide sample data for the threshold intensity in Table II for reference. In a certain sense, the growth rate suppression is related to the dimensionality of the particle trajectories in the cascade. Thus, the migration of charges in auxiliary directions from the cascading region reduces the cascade multiplicity. However, if it was possible to confine the particle motion in the plane where the electric field is maximal, the particle yield would become higher or, alternatively, the cascade threshold would lower. This aspect can be useful for designing future experiments, e.g. to find the optimal setup, geometry, and/or targets that allow to trap particles (e.g. by using plasma shutters [108]).

At fields as high as $E_0 \gtrsim \alpha E_S$, migration becomes

negligible for both the infinite standing wave and focused Gaussian beam configurations. The corresponding growth rates match the result for a uniform rotating E -field (see Fig. 5). First, this is simply because the cascade reaches the exponential phase at a sub-cycle time before particles can escape, as $W_{\text{cr}}T \gg 1$. Second, the migration rate decreases as the field strength increases, meaning that the particles are trapped in the antinode center, where the electric field is maximal. This resembles the anomalous radiative trapping effect found for electrons moving in a linearly polarized standing wave [109] and in dipole waves [41, 110]. As a consequence, at a high field, the model of a cascade in a rotating uniform electric field is universal for all the CP standing wave-like fields.

Our model provides the explicit scaling of the particle number growth rate with the field strength [see Eq. (32)]. It significantly improves the previous findings of [40, 43, 45, 46, 78] (summarized in Table I). The scaling $\Gamma \propto E_0^{1/4}$ proposed in Ref. [40] reappears in our formula (32) at $E_0 \gg \alpha E_S$, however, we showed that it sets in only beyond the critical field of QED E_S , namely, where the applicability of the cascade model is debatable.

With our model, we also estimate the threshold at which plasma effects and backreaction become relevant. At the single laser intensity $I \approx 2 \times 10^{24}$ W/cm² (in a two-beam setup) the produced electron-positron plasma can reach the critical density in one field cycle, meaning that some collective effects could be observable. At intensities $I \gtrsim 10^{25}$ W/cm², the external field can be fully screened after one cycle. In general, the density of the produced plasma is well-controllable by tuning the laser intensity. Once available in the laboratory, avalanche-type cascades will open a path to studying relativistic e^-e^+ plasma, relevant to astrophysical phenomena.

In this work, we focused on the case of a circularly polarized standing wave, as this field is favorable for the cascade onset and formation of the steady state. The cascades in such a field are also tractable with a theoretical approach. However, linearly polarized fields are easier to access experimentally. Also, it was proposed that using the linear polarization can be more beneficial at lower field strength near the cascade onset threshold [47]. This is due to the properties of particle motion at the time scale of the field period. However, in linearly polarized fields, the cascade steady state cannot extend for longer than one field period, and hence circular polarization should provide higher particle yield at higher fields. The full comparative study for both polarizations, as well as the generalization to single and multiple tightly focused laser beams and structured laser pulses (e.g. Laguerre-Gauss modes), is under progress and left for future work.

Finally, let us make some additional remarks. Our goal was to derive the cascade growth rate scaling with the field strength, therefore, we disregarded the Sauter-Schwinger pair creation from vacuum for the sake of clarity, which might be important in the high-field limit

[26, 40, 90]. For a realistic simulation at ultra-high intensities, this effect should be accounted for in future studies. Nevertheless, the cascade growth rate should not be affected by the spontaneous pair production as long as the field is not screened. Hence, we believe that the presented results are physically relevant and, moreover, can be used to refine the threshold for attainable laser intensities [40].

ACKNOWLEDGEMENTS

We express our gratitude to A.M. Fedotov, E.G. Gelfer, A. Gonoskov, T. Grismayer and M. Vranic for fruitful and elucidating discussions. This work used the open-source PIC code SMILEI, the authors are grateful to all SMILEI contributors and to the SMILEI-dev team for its support. Simulations were performed on the Irene-Joliot-Curie machine hosted at TGCC, France, using High-Performance Computing resources from GENCI-TGCC (Grant No. A0030507678). This work received financial support from the French state agency *Agence Nationale de la Recherche*, in the context of the *Investissements d'Avenir* program (reference ANR-18-EURE-0014). A.A.M. was supported by Sorbonne Université in the framework of the Initiative Physique des Infinis (IDEX SUPER).

Appendix A: Small-time dynamics of e^\pm in a cascade

Let us discuss the motion of electrons in between emissions of photons in a cascade developing in a general field, which varies in time and space with the characteristic frequency ω and the corresponding wavelength λ . We follow Ref. [42] and provide only the details necessary for the current work.

Consider an electron that is initially located at the origin at time $t = 0$ in an external field. The electric and magnetic fields at the initial position are characterized by the EM field tensor $F^{\mu\nu} = F^{\mu\nu}(0)$ combining the electric \mathbf{E} and magnetic \mathbf{B} components. As mentioned in Section II, we assume that the electron motion is semiclassical, meaning that it is governed by the Lorentz equations:⁹

$$\frac{dp^\mu}{d\tau} = -\frac{e}{mc} F^\mu{}_\nu(x(\tau))p^\nu, \quad p_\mu(0) = p_\mu^{(0)}, \quad (\text{A1})$$

where p^μ and x^μ are the 4-momentum and time-space coordinate of the electron and τ is the proper time.¹⁰ To solve this equation we impose the following assumptions:

- (i) the time between photon emissions is small, hence, we consider time intervals $t \ll \omega^{-1}$. The electron propagates almost as in a constant field $F_{\mu\nu}(0)$, the corrections are provided by the field derivatives, $F_{\mu\nu,\sigma}(0) \equiv \partial F_{\mu\nu}(0)/\partial x^\sigma$;
- (ii) due to acceleration by the field, e^- rapidly becomes ultra-relativistic at time scale $mc/eE \ll t$;
- (iii) energy gained by e^- during acceleration is much higher than the initial energy, $eEt/mc \gg \gamma_e(0)$;
- (iv) The field is of electric type, namely, $E > B$ (this is a wide class of fields, and the field of the electric antinode of a CP standing wave belongs to it).

When solving the equations of motion, it is convenient to use the proper reference frame of the field, where the electric and magnetic fields are parallel (or at least one of them vanishes), and their magnitude is given by the invariants:

$$\epsilon = \sqrt{\sqrt{\mathcal{F}^2 + \mathcal{G}^2} + \mathcal{F}}, \quad (\text{A2})$$

$$\eta = \sqrt{\sqrt{\mathcal{F}^2 + \mathcal{G}^2} - \mathcal{F}} \quad (\text{A3})$$

where $\mathcal{F} = (\mathbf{E}^2 - c^2\mathbf{B}^2)/2$ and $\mathcal{G} = c\mathbf{B} \cdot \mathbf{E}$ are the field invariants. Mathematically, $\alpha_k = \{\epsilon, -\epsilon, i\eta, -i\eta\}$ are the eigenvalues of the field tensor $F^\mu{}_\nu(0)$ with u_k^μ being the corresponding eigenvectors:

$$F(0)u_k = \frac{\alpha_k}{c}u_k, \quad k = 1, \dots, 4. \quad (\text{A4})$$

The solution to Eq. (A1) at the 0th order in $\omega t \ll 1$ can be expanded in four terms $\propto u_k e^{e\alpha_k \tau/mc}$. However, in the field of electric type $\epsilon > 0$ and $\epsilon > \eta$. At $\tau > mc/e\epsilon$, the dominating contribution corresponds to $\propto u_1 e^{e\epsilon \tau/mc}$, and the solution simplifies (see Ref. [42] for more details). The eigenvector u_1 can be expressed in terms of the laboratory frame field components:

$$u_1^\mu = \left(1, \frac{c^2(\mathbf{E} \cdot \mathbf{B})\mathbf{B} + \epsilon c[\mathbf{E} \times \mathbf{B}] + \epsilon^2 \mathbf{E}}{\epsilon(c^2 B^2 + \epsilon^2)} \right). \quad (\text{A5})$$

It is worth noting that, although ϵ represents the electric field strength in the proper frame of the field, in the laboratory frame this quantity depends both on the electric and magnetic components.

Under the above listed conditions, we solve Eq. (A1) to the order $O((\omega t)^3)$ to find the key parameters:

$$\gamma_e(t) \simeq \frac{e\epsilon t}{mc}, \quad (\text{A6})$$

$$\chi_e^2(t) \simeq \chi_e^2(0) + \left(\frac{\hbar e^2 \epsilon^2 \omega_{\text{eff}} t^2}{m^3 c^4} \right)^2, \quad (\text{A7})$$

where $\chi_e(0) = e\hbar \sqrt{-(p_\mu^{(0)} F^{\mu\nu}(0))^2/m^3 c^4}$, and ω_{eff} is defined by

$$\omega_{\text{eff}}^2 = F_{\mu\nu,\sigma}(0)u_1^\mu u_1^\sigma (J^{-1})^\nu{}_\lambda F^\lambda{}_{\kappa,\rho}(0)u_1^\rho u_1^\kappa, \quad (\text{A8})$$

⁹ The discussion of positron motion will be the same except the change of sign in the RHS of Eq. (A1).

¹⁰ In our notations, after every quantum event, an electron is assigned new initial conditions (this includes scattered electrons in the Compton process).

$$J = \left(2\frac{\epsilon}{c}\mathbf{1} - F(0)\right)^2, \quad (\text{A9})$$

The initial value of the χ -parameter in Eq. (A7) can be omitted too as the second term rapidly becomes dominating at the time scales of interest for us. As a result, we get Eqs. (8), (9). We remark here that the combination $\omega_{\text{eff}}t^2$ is Lorentz invariant, and hence Eq. (A7).

Appendix B: Electron dynamics and cascade growth rate in asymptotically weak and strong fields

For reference purposes, we collect all the asymptotic expressions in the low- and high-field regimes with full numerical coefficients for the quantities introduced in the main text.

The full probability rates of photon emission and e^-e^+ pair creation are given by:

$$W_{\text{cs}}(\gamma_e, \chi_e) \simeq \begin{cases} \frac{5}{2\sqrt{3}} \frac{\alpha\chi_e}{\tau_C\gamma_e}, & \chi_e \ll 1, \\ \frac{14\Gamma(2/3)}{3^{7/3}} \frac{\alpha\chi_e^{2/3}}{\tau_C\gamma_e}, & \chi_e \gg 1, \end{cases} \quad (\text{B1})$$

$$W_{\text{bw}}(\gamma_\gamma, \chi_\gamma) \simeq \begin{cases} \sqrt{\frac{3}{2}} \frac{3}{16} \frac{\alpha\chi_\gamma}{\tau_C\gamma_\gamma} e^{-8/3\chi_\gamma}, & \chi_\gamma \ll 1, \\ \frac{3^{5/3}5\Gamma^4(2/3)}{28\pi^2} \frac{\alpha\chi_\gamma^{2/3}}{\tau_C\gamma_\gamma}, & \chi_\gamma \gg 1. \end{cases} \quad (\text{B2})$$

We used Eq. (B1) to calculate the asymptotic values for t_{em} , γ_{em} , and χ_{em} as described in Section II C. Thus, the time of emission reads:

$$t_{\text{em}} \simeq \begin{cases} \frac{2 \cdot \sqrt[4]{3}}{\sqrt{5}\alpha} \sqrt{\frac{\tau_C\alpha E_S}{\omega_{\text{eff}}\epsilon}}, & \chi_{\text{em}} \ll 1, \\ \frac{3}{\alpha} \left(\frac{2}{7\Gamma(2/3)}\right)^{3/4} \sqrt{\frac{\tau_C}{\omega_{\text{eff}}}} \left(\frac{\alpha E_S}{\epsilon}\right)^{1/4}, & \chi_{\text{em}} \gg 1. \end{cases} \quad (\text{B3})$$

Here, ϵ is the invariant field strength as defined in Eq. (A2), and ω_{eff} is given by Eq. (A8). The values for γ_{em} and χ_{em} are obtained straightforwardly by substituting t_{em} to Eqs. (8)-(9):

$$\gamma_{\text{em}} \simeq \begin{cases} \frac{2 \cdot \sqrt[4]{3}}{\sqrt{5}} \sqrt{\frac{\epsilon}{\omega_{\text{eff}}\tau_C\alpha E_S}}, & \chi_{\text{em}} \ll 1, \\ \frac{3}{\sqrt{\omega_{\text{eff}}\tau_C}} \left[\frac{2}{7\Gamma(2/3)} \frac{\epsilon}{\alpha E_S}\right]^{3/4}, & \chi_{\text{em}} \gg 1, \end{cases} \quad (\text{B4})$$

$$\chi_{\text{em}} \simeq \begin{cases} \frac{4\sqrt{3}}{5} \frac{\epsilon}{\alpha E_S}, & \epsilon \ll \alpha E_S, \\ 9 \left[\frac{2}{7\Gamma(2/3)} \frac{\epsilon}{\alpha E_S}\right]^{3/2}, & \epsilon \gg \alpha E_S. \end{cases} \quad (\text{B5})$$

Note that in the last equation, we express the asymptotic conditions in terms of the invariant field ϵ , so that they are consistent with the initial hypothesis $\chi_{\text{em}} \ll 1$ or $\chi_{\text{em}} \gg 1$, respectively. The threshold $\epsilon = \alpha E_S \approx E_S/137$ separates the regimes of the avalanche-type cascade development.

The effective emission probability rate $W_{\text{rad}} = W_{\text{cs}}(\gamma_{\text{em}}, \chi_{\text{em}})$ at t_{em} at asymptotically low and high fields can be expressed as (see the corresponding discussion in Section III B):

$$W_{\text{cs}}(\gamma_{\text{em}}, \chi_{\text{em}}) \simeq \frac{\alpha}{\tau_C} \times \begin{cases} \frac{\sqrt{5}}{\sqrt[4]{3}} \sqrt{\frac{\epsilon\omega_{\text{eff}}\tau_C}{\alpha E_S}}, & \epsilon \ll \alpha E_S, \\ \frac{\sqrt{2}}{9} [14\Gamma(2/3)]^{3/4} \sqrt{\omega_{\text{eff}}\tau_C} \left(\frac{\epsilon}{\alpha E_S}\right)^{1/4}, & \epsilon \gg \alpha E_S. \end{cases} \quad (\text{B6})$$

Finally, we collect the asymptotic expressions for the particle growth rate derived and discussed in Section III C

and the used numerical coefficients:

$$\Gamma(\epsilon) \simeq \frac{\alpha}{\tau_C} \times \begin{cases} \frac{9\sqrt{5}\Gamma^4(2/3)}{14^{1/2}\sqrt{3}\pi^2} \sqrt{\frac{\epsilon\omega_{\text{eff}}\tau_C}{\alpha E_S}} \left[\frac{2\sqrt{5}}{\sqrt[4]{3}} \frac{\alpha}{\nu} \sqrt{\frac{\epsilon\omega_{\text{eff}}\tau_C}{\alpha E_S}} - 1 \right] \exp\left(-\frac{10\alpha E_S}{3\sqrt{3}\epsilon}\right), & \epsilon \ll \alpha E_S, \nu > 0, \\ \frac{3^{5/6}\sqrt{5}}{\sqrt{7}\pi} \Gamma^2(2/3) \sqrt{\frac{\epsilon\omega_{\text{eff}}\tau_C}{\alpha E_S}} \exp\left(-\frac{5\alpha E_S}{3\sqrt{3}\epsilon}\right), & \epsilon \ll \alpha E_S, \nu = 0, \\ c_1 \frac{\epsilon}{\alpha E_S} \left[\sqrt{1 + c_2 \sqrt{\omega_{\text{eff}}\tau_C} \left(\frac{\alpha E_S}{\epsilon}\right)^{3/4}} - 1 \right], & \alpha E_S < \epsilon < c_3 \alpha (\omega_{\text{eff}}\tau_C)^{2/3}, \\ \frac{2\sqrt{2}}{9} [14\Gamma(2/3)]^{3/4} \sqrt{\omega_{\text{eff}}\tau_C} \left(\frac{\epsilon}{\alpha E_S}\right)^{1/4}, & c_3 \alpha (\omega_{\text{eff}}\tau_C)^{2/3} \ll \epsilon. \end{cases} \quad (\text{B7})$$

$$c_1 = \frac{\tau_C W_{\text{BW}}(1,1)}{2} \approx 0.516 \times 10^{-4}, \quad (\text{B8})$$

$$c_2 = \frac{8\sqrt{2} (14\Gamma(2/3))^{3/4}}{9\tau_C W_{\text{BW}}(1,1)} \approx 1.107 \times 10^5, \quad (\text{B9})$$

$$c_3 = \left(\frac{2}{3}\right)^{2/3} \frac{224\Gamma(2/3)}{9(\tau_C W_{\text{BW}}(1,1))^{4/3}} \approx 5.31 \times 10^6, \quad (\text{B10})$$

$$\tau_C W_{\text{BW}}(1,1) \approx 1.0318068870 \times 10^{-4}. \quad (\text{B11})$$

Appendix C: Particle number equations in quasi-steady state

Cascade equations in general form read

$$\left[\frac{\partial}{\partial t} + \frac{c^2 \mathbf{p}_e}{\varepsilon_e} \cdot \frac{\partial}{\partial \mathbf{r}} \pm \frac{\partial}{\partial \mathbf{p}_e} \cdot \mathbf{F}_L \right] f_{\pm}(\mathbf{r}, \mathbf{p}_e, t) = \int d\mathbf{p}_\gamma W_{\text{rad}}(\mathbf{p}_e + \mathbf{p}_\gamma \rightarrow \mathbf{p}_\gamma) f_{\pm}(\mathbf{r}, \mathbf{p}_e + \mathbf{p}_\gamma, t) - W_{\text{rad}}(\mathbf{p}_e) f_{\pm}(\mathbf{r}, \mathbf{p}_e, t) + \int d\mathbf{p}_\gamma W_{\text{cr}}(\mathbf{p}_\gamma \rightarrow \mathbf{p}_e) f_\gamma(\mathbf{r}, \mathbf{p}_\gamma, t), \quad (\text{C1})$$

$$\left[\frac{\partial}{\partial t} + \frac{c^2 \mathbf{p}_\gamma}{\varepsilon_\gamma} \cdot \frac{\partial}{\partial \mathbf{r}} \right] f_\gamma(\mathbf{r}, \mathbf{p}_\gamma, t) = \int d\mathbf{p}_e W_{\text{cr}}(\mathbf{p}_e \rightarrow \mathbf{p}_\gamma) [f_-(\mathbf{r}, \mathbf{p}_e, t) + f_+(\mathbf{r}, \mathbf{p}_e, t)] - W_{\text{cr}}(\mathbf{p}_\gamma) f_\gamma(\mathbf{r}, \mathbf{p}_\gamma, t), \quad (\text{C2})$$

where $f_a(\mathbf{r}, \mathbf{p}, t)$, $a = \{\pm, \gamma\}$, are the electron, positron, and photon distribution functions. The LHS of the equations describes the continuous dynamics of particles with momenta $\mathbf{p}_{e,\gamma}$ and energies $\varepsilon_{e,\gamma}$ for e^\pm and γ , respectively; $\pm \mathbf{F}_L = \pm e(\mathbf{E} + c^2 \mathbf{p}_e \times \mathbf{B}/\varepsilon_e)$ is the Lorentz force acting on a charged particle. In the RHS, we collect the source terms corresponding to the stochastic processes of photon emission and pair creation, where $W_{\text{rad}}(\mathbf{p}_e \rightarrow \mathbf{p}_\gamma)$ is the differential probability rate for an electron or positron with momentum \mathbf{p}_e to emit a photon with momentum \mathbf{p}_γ , and $W_{\text{cr}}(\mathbf{p}_\gamma \rightarrow \mathbf{p}_e)$ is the differential probability rate for a photon with momentum \mathbf{p}_γ to create a pair such that e^- or e^+ gets momentum \mathbf{p}_e . Equations (C1) and (C2) provide a starting point to model QED cascades in various scenarios, including electromagnetic air showers [31], shower-type cascades in interaction of high-energy beams with laser pulses [33], and avalanche-type cascades [43, 62]. Let us point

out here that the probability rates depend on the field strength, which in turn can depend on \mathbf{r} and t , namely, $W_{\text{cr,rad}}(\mathbf{p}_a \rightarrow \mathbf{p}_b) \equiv W_{\text{cr,rad}}(\mathbf{p}_a \rightarrow \mathbf{p}_b; \mathbf{E}(\mathbf{r}, t), \mathbf{B}(\mathbf{r}, t))$, $W_{\text{cr,rad}}(\mathbf{p}_a) \equiv W_{\text{cr,rad}}(\mathbf{p}_a; \mathbf{E}(\mathbf{r}, t), \mathbf{B}(\mathbf{r}, t))$. Within the LCFA, the fields enter through the quantum parameter $\chi_{e,\gamma}$ of the incoming particle [see Eq. (1)]. For brevity, we omit the explicit field dependence in our notation.

Let us consider an avalanche-type e^- -seeded cascade developing in an electric antinode of a standing wave, formed by two circularly polarized waves propagating along the z -axis. We assume that e^- is injected close to the E -antinode centered at the origin $\mathbf{r} = 0$. In the triggered cascade, the number of produced pairs can grow exponentially with time, $N_p \sim e^{\Gamma t}$. As the mean free path time of e^\pm and γ in the cascade is small (see Section II), the majority of particles will be created in the small vicinity of the E -antinode centre, which we denote as domain D . To identify the dependence of Γ on the

field parameters, it is therefore enough to study the particle distributions within D . Assuming that the field is

almost homogeneous in D , let us integrate out the coordinate dependence \mathbf{r} . For Eq. (C1), we obtain:

$$\begin{aligned} \frac{\partial}{\partial t} f_{\pm}(\mathbf{p}_e, t) + \frac{c^2 \mathbf{p}_e}{\varepsilon_e} \cdot \int_{\partial D} d\mathbf{S} f_{\pm}(\mathbf{r}, \mathbf{p}_e, t) \pm \frac{\partial}{\partial \mathbf{p}_e} \cdot \int_D d\mathbf{r} \mathbf{F}_L f_{\pm}(\mathbf{r}, \mathbf{p}_e, t) \\ = \int d\mathbf{p}_\gamma W_{\text{rad}}(\mathbf{p}_e + \mathbf{p}_\gamma \rightarrow \mathbf{p}_\gamma) f_{\pm}(\mathbf{p}_e + \mathbf{p}_\gamma, t) \\ - W_{\text{rad}}(\mathbf{p}_e) f_{\pm}(\mathbf{p}_e, t) + \int d\mathbf{p}_\gamma W_{\text{cr}}(\mathbf{p}_\gamma \rightarrow \mathbf{p}_e) f_\gamma(\mathbf{p}_\gamma, t), \end{aligned} \quad (\text{C3})$$

where we introduced

$$f_{\pm, \gamma}(\mathbf{p}_e, t) = \int_D d\mathbf{r} f_{\pm, \gamma}(\mathbf{r}, \mathbf{p}_e, t).$$

Here, to simplify the RHS, we approximate the field dependence of the probability rates by a uniform field that corresponds to the field at the E -antinode centre, $W_{\text{cr, rad}}(\mathbf{p}_a \rightarrow \mathbf{p}_b) \equiv W_{\text{cr, rad}}(\mathbf{p}_a \rightarrow \mathbf{p}_b; \mathbf{E}(0, t), \mathbf{B}(0, t))$. For the second term in the LHS, we used the divergence theorem to cast it into the surface integral. It accounts for the particle flux through the surface ∂D . The flux can be caused by the migration of charged particles in the direction of the electric field gradient, in our case to the B -antinodes (see Fig. 4). As we consider waves that are infinite in the transverse plane, particles migrate only in the longitudinal direction. However, Eq. (C3) can be generalised straightforwardly to account for migration in other directions for other field configurations, e.g. focused laser fields.

In the events of emission or pair creation, the incoming and outgoing particles are ultrarelativistic, thus $\varepsilon_e \approx c|\mathbf{p}_e|$. Following [43, 62], we assume that in each quantum process the momenta of the initial and secondary particles are collinear:

$$\begin{aligned} W_{\text{rad}}(\mathbf{p}_e \rightarrow \mathbf{p}_\gamma) &= \int_0^1 d\lambda \delta(\mathbf{p}_\gamma - \lambda \mathbf{p}_e) \varepsilon_e \left. \frac{dW_{\text{rad}}(\mathbf{p}_e, \varepsilon_\gamma)}{d\varepsilon_\gamma} \right|_{\varepsilon_\gamma = \lambda \varepsilon_e}, \\ W_{\text{cr}}(\mathbf{p}_\gamma \rightarrow \mathbf{p}_e) &= \int_0^1 d\lambda \delta(\mathbf{p} - \lambda \mathbf{p}_\gamma) \varepsilon_\gamma \left. \frac{dW_{\text{cr}}(\mathbf{p}_\gamma, \varepsilon'_e)}{d\varepsilon'_e} \right|_{\varepsilon'_e = \lambda \varepsilon_\gamma}. \end{aligned}$$

Note that within the LCFA, the probability rates explicitly depend only on the particle energy and χ parameter:

$$\frac{dW_{\text{rad}}(\mathbf{p}_e, \varepsilon_\gamma)}{d\varepsilon_\gamma} = \frac{dW_{\text{rad}}(\varepsilon_e, \chi_e, \varepsilon_\gamma)}{d\varepsilon_\gamma}, \quad \frac{dW_{\text{cr}}(\mathbf{p}_\gamma, \varepsilon_e)}{d\varepsilon_e} = \frac{dW_{\text{cr}}(\varepsilon_\gamma, \chi_\gamma, \varepsilon_e)}{d\varepsilon_e}, \quad (\text{C4})$$

[c.f. Eqs. (2) and (3)].¹¹ By applying this to the RHS of Eq. (C3), we can integrate out the angular dependence in \mathbf{p}_γ . After repeating the same steps for Eq. (C2), we get:

$$\begin{aligned} \frac{\partial}{\partial t} f_{\pm}(\mathbf{p}_e, t) + \frac{c^2 \mathbf{p}_e}{\varepsilon_e} \cdot \int_{\partial D} d\mathbf{S} f_{\pm}(\mathbf{r}, \mathbf{p}_e, t) \pm \frac{\partial}{\partial \mathbf{p}_e} \cdot \int_D d\mathbf{r} \mathbf{F}_L f_{\pm}(\mathbf{r}, \mathbf{p}_e, t) = -W_{\text{rad}}(\mathbf{p}_e) f_{\pm}(\mathbf{p}_e, t) \\ + \int_{\varepsilon_e}^{\infty} d\varepsilon' \frac{\varepsilon'^2}{\varepsilon_e^2} \left[\left. \frac{dW_{\text{rad}}(\mathbf{p}', \varepsilon_\gamma)}{d\varepsilon_\gamma} \right|_{\varepsilon_\gamma = \varepsilon' - \varepsilon_e} f_{\pm}(\mathbf{p}', t) + \frac{dW_{\text{cr}}(\mathbf{p}', \varepsilon_e)}{d\varepsilon_e} f_\gamma(\mathbf{p}', t) \right] \Bigg|_{\mathbf{p}' = \varepsilon' \frac{c\mathbf{p}_e}{\varepsilon_e}}. \end{aligned} \quad (\text{C5})$$

$$\begin{aligned} \frac{\partial}{\partial t} f_\gamma(\mathbf{p}_\gamma, t) &= -W_{\text{cr}}(\mathbf{p}_\gamma) f_\gamma(\mathbf{p}_\gamma, t) \\ &+ \int_{\varepsilon_\gamma}^{\infty} d\varepsilon' \frac{\varepsilon'^2}{\varepsilon_\gamma^2} \frac{dW_{\text{rad}}(\mathbf{p}', \varepsilon_\gamma)}{d\varepsilon_\gamma} [f_-(\mathbf{p}', t) + f_+(\mathbf{p}', t)] \Bigg|_{\mathbf{p}' = \varepsilon' \frac{c\mathbf{p}_\gamma}{\varepsilon_\gamma}}. \end{aligned} \quad (\text{C6})$$

For a uniform field, for example, if $\mathbf{F}_L = e\mathbf{E}(t)$ (this includes a uniform rotating electric field), the flux term in Eq. (C5) vanishes and we recover the equations used in Refs. [43, 62].

¹¹ We use particle energy $\varepsilon_{e, \gamma} = \gamma_{e, \gamma} mc^2$ as the argument for the probability rates to simplify the notations within Appendix C.

The transition to the notation used in Eqs. (2), (3) is straightforward.

As we aim to obtain the equations for particle numbers, we integrate out the particle momenta from Eqs. (C5)-(C6):

$$\frac{\partial}{\partial t} N_{\pm}(t) + \nu_{\pm} N_{\pm}(t) = \int d\mathbf{p}_e \int_{\varepsilon_e}^{\infty} d\varepsilon' \frac{\varepsilon'^2}{\varepsilon_e^2} \frac{dW_{\text{cr}}(\mathbf{p}', \varepsilon_e)}{d\varepsilon_e} f_{\gamma}(\mathbf{p}', t) \Big|_{\mathbf{p}'=\varepsilon' \frac{c\mathbf{p}_e}{\varepsilon_e}}, \quad (\text{C7})$$

$$\frac{\partial}{\partial t} N_{\gamma}(t) = \int d\mathbf{p}_{\gamma} \left\{ -W_{\text{cr}}(\mathbf{p}_{\gamma}) f_{\gamma}(\mathbf{p}_{\gamma}, t) + \int_{\varepsilon_{\gamma}}^{\infty} d\varepsilon' \frac{\varepsilon'^2}{\varepsilon_{\gamma}^2} \frac{dW_{\text{rad}}(\mathbf{p}', \varepsilon_{\gamma})}{d\varepsilon_{\gamma}} [f_{-}(\mathbf{p}', t) + f_{+}(\mathbf{p}', t)] \Big|_{\mathbf{p}'=\varepsilon' \frac{c\mathbf{p}_{\gamma}}{\varepsilon_{\gamma}}} \right\}, \quad (\text{C8})$$

where

$$N_a(t) = \int d\mathbf{p} f_a(\mathbf{p}, t), \quad (\text{C9})$$

$$\mathbf{j}_{\pm}(\mathbf{r}, t) = \int d\mathbf{p}_e \frac{c^2 \mathbf{p}_e}{\varepsilon_e} f_{\pm}(\mathbf{r}, \mathbf{p}_e, t), \quad (\text{C10})$$

$$\nu_{\pm}(t) = \frac{1}{N_{\pm}(t)} \int_{\partial D} d\mathbf{S} \mathbf{j}_{\pm}(\mathbf{r}, t) \quad (\text{C11})$$

are the particle numbers, flows, and effective migration rates, respectively. As the electric field is symmetric around the E -antinode center, we put $\nu_{-}(t) = \nu_{+}(t) \equiv \nu(t)$. Note that in Eq. (C7) we used that

$$\int d\mathbf{p}_e \left\{ \int_{\varepsilon}^{\infty} d\varepsilon' \frac{\varepsilon'^2}{\varepsilon_e^2} \left[\frac{dW_{\text{rad}}(\mathbf{p}', \varepsilon_{\gamma})}{d\varepsilon_{\gamma}} \Big|_{\varepsilon_{\gamma}=\varepsilon'-\varepsilon_e} f_{\pm}(\mathbf{p}', t) \right] \Big|_{\mathbf{p}'=\varepsilon' \frac{c\mathbf{p}_e}{\varepsilon_e}} - W_{\text{rad}}(\mathbf{p}_e) f_{\pm}(\mathbf{p}_e, t) \right\} = 0,$$

which can be shown by interchanging the integrals in the first term and noticing that $dW_{\text{rad}}(\mathbf{p}', \varepsilon_{\gamma} - \varepsilon_e)/d\varepsilon_{\gamma} = -dW_{\text{rad}}(\mathbf{p}', \varepsilon_{\gamma} - \varepsilon_e)/d\varepsilon_e$ under the integral. Physically, it corresponds to the balance of radiation.

To simplify the equations further, let us consider the following term in the RHS of Eq. (C8):

$$\int d\mathbf{p}_{\gamma} \int_{\varepsilon_{\gamma}}^{\infty} d\varepsilon' \frac{\varepsilon'^2}{\varepsilon_{\gamma}^2} \frac{dW_{\text{rad}}(\mathbf{p}', \varepsilon_{\gamma})}{d\varepsilon_{\gamma}} f_{\pm}(\mathbf{p}', t) \Big|_{\mathbf{p}'=\varepsilon' \frac{c\mathbf{p}_{\gamma}}{\varepsilon_{\gamma}}} \quad (\text{C12})$$

It is convenient to pass to spherical coordinates in momentum space, $\mathbf{p}_a \rightarrow \{\varepsilon_a/c, \mathbf{n}_a\}$, where $\mathbf{n}_a = \mathbf{p}_a/|\mathbf{p}_a|$ is the unit vector. The emission collinearity condition $\mathbf{p}' = \varepsilon' \frac{c\mathbf{p}_{\gamma}}{\varepsilon_{\gamma}}$ simply means that the integration over \mathbf{n}_{γ} in the outer integral can be replaced by \mathbf{n}' :

$$\frac{1}{c^3} \int_0^{\infty} d\varepsilon_{\gamma} d\mathbf{n}' \varepsilon_{\gamma}^2 \int_{\varepsilon_e}^{\infty} d\varepsilon' \frac{\varepsilon'^2}{\varepsilon_{\gamma}^2} \frac{dW_{\text{rad}}(\varepsilon', \chi', \varepsilon_{\gamma})}{d\varepsilon_{\gamma}} f_{\pm}(\varepsilon', \mathbf{n}', t), \quad (\text{C13})$$

Note that we wrote the argument of $dW_{\text{rad}}/d\varepsilon_{\gamma}$ so that it corresponds to Eq. (C4), and χ' depends on \mathbf{n}' (e.g. in the reference frame co-moving with the electric field component [62]). Now we can interchange the $d\varepsilon_{\gamma}$ and $d\varepsilon'$ integrals:

$$\frac{1}{c^3} \int_0^{\infty} d\varepsilon' d\mathbf{n}' \varepsilon'^2 f_{\pm}(\varepsilon', \mathbf{n}', t) \int_0^{\varepsilon'} d\varepsilon_{\gamma} \frac{dW_{\text{rad}}(\varepsilon', \chi', \varepsilon_{\gamma})}{d\varepsilon_{\gamma}} \quad (\text{C14})$$

The rightmost integral gives $W_{\text{rad}}(\varepsilon', \chi')$, and the whole expression can be written in a compact form:

$$\int d\mathbf{p}' W_{\text{rad}}(\mathbf{p}') f_{\pm}(\mathbf{p}', t). \quad (\text{C15})$$

After repeating the same steps for the RHS of Eq. (C7), we can rewrite the particle number equations as follows:

$$\frac{\partial}{\partial t} N_{\pm}(t) = -\nu(t) N_{\pm}(t) + W_{\text{cr}}(t) N_{\gamma}(t), \quad (\text{C16})$$

$$\frac{\partial}{\partial t} N_{\gamma}(t) = W_{\text{rad}}(t) [N_{-}(t) + N_{+}(t)] - W_{\text{cr}}(t) N_{\gamma}(t), \quad (\text{C17})$$

where we introduced time-dependent effective rates:

$$W_{\text{rad}}(t) = \frac{1}{N_{-}(t) + N_{+}(t)} \int d\mathbf{p}' W_{\text{rad}}(\mathbf{p}') [f_{-}(\mathbf{p}', t) + f_{+}(\mathbf{p}', t)], \quad (\text{C18})$$

$$W_{\text{cr}}(t) = \frac{1}{N_\gamma(t)} \int d\mathbf{p}' W_{\text{cr}}(\mathbf{p}') f_\gamma(\mathbf{p}', t). \quad (\text{C19})$$

Recall that, here, the probability rates also depend on time, $W_{\text{rad,cr}}(\mathbf{p}') \equiv W_{\text{rad,cr}}(\mathbf{p}'; \mathbf{E}(0, t), \mathbf{B}(0, t))$. For a cascade developing at the E -antinode center of a CP standing wave, the probability rates are independent of time in the frame co-rotating with the electric field. Transition to such the frame can be done for Eqs. (C1), (C2) (see Ref. [62]), however, does not change the form of Eqs. (C16), (C17).

To advance, we assume now that the cascade rapidly reaches the (quasi)-steady state, and that the time dependence in f_a factorizes in the frame co-rotating with the electric field: $f_a(\mathbf{p}_a, t) = f_a(\mathbf{p}_a)g_a(t)$ [anticipating that $g_a(t) \sim e^{\Gamma t}$]. We use the probabilities in the LCFA, so $W_{\text{rad}}(\mathbf{p}') = W_{\text{rad}}(\varepsilon', \chi')$, $W_{\text{cr}}(\mathbf{p}') = W_{\text{cr}}(\varepsilon', \chi')$, hence, χ' can be used as an independent integration variable in Eqs. (C18), (C19). Passing to the new variables $\mathbf{p}' \rightarrow \{\varepsilon', \chi', \theta'\}$ casts the distribution function to

$$f_\pm(\mathbf{p}') d\mathbf{p}' = \tilde{f}_\pm(\varepsilon', \chi', \theta') d\varepsilon' d\chi' \sin\theta' d\theta', \quad (\text{C20})$$

where $-\pi/2 < \theta' \leq \pi/2$ is the azimuthal angle in the system such that the electric field rotates in the plane $\theta' = 0$. As a result of the distribution function factorisation $g_a(t)$ cancels out in Eqs. (C18), (C19) [with $N_a(t)$ written explicitly, see Eq. (C9)], and the effective rates become stationary:

$$W_{\text{rad}} = \frac{\int d\varepsilon' d\chi' \sin\theta' d\theta' W_{\text{rad}}(\varepsilon', \chi') [\tilde{f}_-(\varepsilon', \chi', \theta') + \tilde{f}_+(\varepsilon', \chi', \theta')]}{\int d\varepsilon' d\chi' \sin\theta' d\theta' [\tilde{f}_-(\varepsilon', \chi', \theta') + \tilde{f}_+(\varepsilon', \chi', \theta')]}, \quad (\text{C21})$$

$$W_{\text{cr}} = \frac{\int d\varepsilon' d\chi' \sin\theta' d\theta' W_{\text{cr}}(\varepsilon', \chi') \tilde{f}_\gamma(\varepsilon', \chi', \theta')}{\int d\varepsilon' d\chi' \sin\theta' d\theta' \tilde{f}_\gamma(\varepsilon', \chi', \theta')}. \quad (\text{C22})$$

We can apply the same reasoning to the migration rate, $\nu(t) \rightarrow \nu$, see Eq. (C11). By using these expressions in Eqs. (C16), (C17), we finally arrive at the particle number equations in the steady state:

$$\frac{dN_\pm(t)}{dt} = W_{\text{cr}}N_\gamma(t) - \nu N_\pm(t), \quad (\text{C23})$$

$$\frac{dN_\gamma(t)}{dt} = W_{\text{rad}}[N_-(t) + N_+(t)] - W_{\text{cr}}N_\gamma(t). \quad (\text{C24})$$

By introducing $N_p = (N_- + N_+)/2$ we cast these relations into Eqs. (18)-(19). At $\nu = 0$, we get the equations of the form used in Refs. [45, 46, 61].

The effective rate of photon emission given in Eqs. (C21) can be simplified further if we take into account the electron dynamics. Let us consider the integral:

$$\int d\varepsilon' d\chi' \sin\theta' d\theta' W_{\text{rad}}(\varepsilon', \chi') \tilde{f}_\pm(\varepsilon', \chi', \theta')$$

The short-time expressions (8)-(9) relate ε_e and χ_e as they are parametrised. We can express χ_e in terms of ε_e : $\chi_e(\varepsilon_e) = (\varepsilon_e^2/mc^2)^2 \omega_{\text{eff}} \tau_C$, meaning that the distribution function can be written as

$$\tilde{f}_\pm(\varepsilon', \chi', \theta') = \tilde{f}_\pm(\varepsilon', \theta') \delta(\chi' - \chi_e(\varepsilon')). \quad (\text{C25})$$

Notably, in the uniform rotating electric field configuration, we can make an additional simplification:

$\tilde{f}_\pm(\varepsilon', \theta') = \tilde{f}_\pm(\varepsilon') \delta(\theta') / \sin\theta'$. Then the integral reads

$$\int d\varepsilon' \sin\theta' d\theta' W_{\text{rad}}(\varepsilon', \chi_e(\varepsilon')) \tilde{f}_\pm(\varepsilon', \theta').$$

In Section III B, we propose to approximate the rate in this integral by a constant $W_{\text{rad}}(\varepsilon', \chi_e(\varepsilon')) \approx W_{\text{cs}}(\gamma_{\text{em}}, \chi_{\text{em}})$, where $\chi_{\text{em}} = \chi_e(\gamma_{\text{em}} mc^2)$. Then the effective rate in Eq. (C21) simplifies to $W_{\text{rad}} \approx W_{\text{cs}}(\gamma_{\text{em}}, \chi_{\text{em}})$.

Developing a similar line of reasoning applied to the RHS of Eq. (C22), requires coupling ε_γ and χ_γ . Since photons propagate along straight lines, and their energy is not altered, let us estimate $\chi_\gamma(\varepsilon_\gamma) \sim \sin(\theta_\gamma) \varepsilon_\gamma / (E_S mc^2)$, where θ_γ is some characteristic angle between the photon momentum and the electric field direction. Then we can rewrite the photon distribution function as in Eq. (C25), substitute it into the effective rate (C22), and obtain $W_{\text{cr}} \approx W_{\text{bw}}(\varepsilon_\gamma / (mc^2), \sin(\theta_\gamma) \varepsilon_\gamma / (E_S mc^2))$. Here, $\sin(\theta_\gamma)$ can be used as a fitting parameter when comparing the resulting growth rate expressions to numerical data.

Let us make several remarks. First, our derivation shows that the steady-state hypothesis is equivalent to taking the limit $W_{\text{rad,cr}}(t \rightarrow \infty) \rightarrow W_{\text{rad,cr}}$. The solution of the steady-state equations for the particle numbers is exponential in time, as we discuss in Section III. In the derivation, we showed that the steady-state naturally arises if the distribution function time dependence fac-

torizes at large times, namely, we can replace the steady-state hypothesis with the latter statement.

Second, the particular time required for this limit to set in, i.e. the steady state formation time, depends on the particular field configuration and its parameters. As of now, the formation of the steady distribution has to be confirmed with numerical simulations for each field configuration, which was done in the past works [42, 43, 45, 47, 48] and the present study. A rigorous proof of the steady state existence would be very interesting, as well as the calculation of the relaxation time, and a systematic classification of the field configurations allowing such a state.

Third, Eqs. (C21)-(C24) are derived in the context of the CP standing wave configuration, and particularly the cascade development at the E -antinode center, where the field simplifies to a rotating E -field. However, these expressions can be generalized to cascades in other field configurations that allow a steady state.

And last, to calculate the cascade particle growth rate Γ , it is enough to solve Eqs. (C23)-(C24). However, the effective rates $W_{\text{rad,cr}}$ and the migration coefficient ν are defined via the distribution functions, which are unknown *a priori*. While solving the full distribution function analytically is intricate, the rates can be estimated under additional approximations, as we propose in Sec. III B, or extracted from numerical simulations, as we do in Sec. IV.

Appendix D: The model of Grismayer et al [45]

The cascade growth rate model proposed by Grismayer et al [45] [see Eqs. (9)–(10) therein] for the rotating E -field was advancing the models of Fedotov et al [40] and Bashmakov et al [46]. The improvement was achieved by reconsidering the assumption that almost all of the energy of a radiating electron is transferred to a photon. Instead, the electron radiation spectrum $dW_{\text{cs}}/d\chi_\gamma$ with $0 < \chi_\gamma < \chi_e$ was fully accounted for in Ref. [45]. At the same time, Grismayer et al follow the preceding works by assuming that the electron mean free path time is given by $t_e \sim W_{\text{rad}}^{-1}$:

$$W_{\text{rad}} \equiv W_{\text{cs}}(\bar{\gamma}_e, \bar{\chi}_e) = \int_0^{\bar{\chi}_e} d\chi_\gamma \frac{dW_{\text{cs}}(\bar{\gamma}_e, \bar{\chi}_e, \chi_\gamma)}{d\chi_\gamma},$$

$$\int_{\varepsilon_\gamma}^{\infty} d\varepsilon' \frac{\varepsilon'^2}{\varepsilon_\gamma^2} \frac{dW_{\text{rad}}(\mathbf{p}', \varepsilon_\gamma)}{d\varepsilon_\gamma} f_{\pm}(\mathbf{p}', t) \approx \frac{N_{\pm}(t)}{4\pi\varepsilon_\gamma^2} \frac{dW_{\text{cs}}(\bar{\gamma}_e, \bar{\chi}_e, \varepsilon_\gamma)}{d\varepsilon_\gamma}, \quad (\text{D3})$$

where we used that $\mathcal{N} \approx 4\pi c^{-3} \bar{\varepsilon}_e^2 e^{g(\bar{\varepsilon}_e)} \sqrt{2\pi/|g''(\bar{\varepsilon}_e)|}$. As a result, we get the equation

$$\frac{\partial}{\partial t} f_\gamma(\mathbf{p}_\gamma, t) = -W_{\text{cr}}(\mathbf{p}_\gamma) f_\gamma(\mathbf{p}_\gamma, t) + \frac{[N_+(t) + N_-(t)]}{4\pi\varepsilon_\gamma^2} \frac{dW_{\text{cs}}(\bar{\gamma}_e, \bar{\chi}_e, \varepsilon_\gamma)}{d\varepsilon_\gamma}, \quad (\text{D4})$$

which can be solved explicitly:

$$f_\gamma(\mathbf{p}_\gamma, t) = \frac{c^3}{4\pi\varepsilon_\gamma^2} \frac{dW_{\text{cs}}(\bar{\gamma}_e, \bar{\chi}_e, \varepsilon_\gamma)}{d\varepsilon_\gamma} \int_0^t dt' [N_+(t') + N_-(t')] e^{-W_{\text{cr}}(\varepsilon_\gamma, \chi_\gamma)(t-t')}. \quad (\text{D5})$$

where $\bar{\gamma}_e$ and $\bar{\chi}_e$ are the characteristic values of γ_e and χ_e at the moment of emission, which depend only on the field parameters. The corresponding model for the number of produced pairs was introduced in Refs. [45, 63] by using a phenomenological approach. We show, how this model arises from the kinetic approach and discuss the approximations that are required to obtain it.

Let us take Eq. (C7) coupled to Eq. (C6) as the starting point. We set the migration term to zero in the context of the uniform rotating electric field model. As in Appendix C, we assume that the cascade reaches the steady state. For Eq. (C7), we repeat the steps proposed in Appendix C, and arrive at:

$$\frac{\partial}{\partial t} N_{\pm}(t) = \int d\mathbf{p}' W_{\text{cr}}(\varepsilon', \chi') f_\gamma(\mathbf{p}', t). \quad (\text{D1})$$

We aim at obtaining a closed equation on $N_{\pm}(t)$. For this, we will use Eq. (C6) to express $f_\gamma(\varepsilon_e, \chi_e, t)$: we approximate the integral over ε' in the RHS in order to pass to the particle numbers $N_{\pm}(t)$, and then integrate the whole equation in time.

As we aim at keeping the differential rate in the expression, $dW_{\text{rad}}/d\chi_\gamma = dW_{\text{cs}}/d\chi_\gamma$, the second integral in the RHS Eq. (C6) can be simplified only by imposing an additional assumption for the distribution functions $f_{\pm}(\mathbf{p}_e, t)$. In the steady state, the normalized electron spectrum does not change with time and has a prominent peak, as was noted by Grismayer et al [45] and confirmed in the current work with numerical simulations. We rewrite the steady-state distribution function in the form:

$$f_{\pm}(\mathbf{p}_e, t) = N_{\pm}(t) \frac{1}{\mathcal{N}} e^{g(\varepsilon_e)}, \quad (\text{D2})$$

where \mathcal{N} normalizes the electron spectrum, $\mathcal{N} = \int d\varepsilon_e e^{g(\varepsilon_e)}$. Let us assume for the moment that $g(\varepsilon_e)$ has a single maximum located at $\bar{\varepsilon}_e$ (see also the discussion below). Therefore, we can use the Laplace method to approximate the integral:

Here, we used the initial condition $f_\gamma(\mathbf{p}_\gamma, 0) = 0$. Finally, after substituting $f_\gamma(\mathbf{p}_\gamma, t)$, putting $W_{\text{cr}} = W_{\text{BW}}$ into Eq. (D1) and rearranging the expression we get:

$$\frac{\partial}{\partial t} N_p(t) = 2 \int_0^t dt' N_p(t') \int_0^{\bar{\chi}_e} d\chi' \frac{dW_{\text{CS}}(\bar{\gamma}_e, \bar{\chi}_e, \chi')}{d\chi'} W_{\text{BW}}(\varepsilon', \chi') e^{-W_{\text{BW}}(\varepsilon', \chi')(t-t')} \quad (\text{D6})$$

where we passed to the number of pairs $N_p = N_- + N_+$, changed the integration variable $\varepsilon' \rightarrow \chi'$, and put the upper limit of the χ' integral as $dW_{\text{CS}}(\bar{\gamma}_e, \bar{\chi}_e, \chi')/d\chi' = 0$ for $\chi' > \bar{\chi}_e$. Following Ref. [45], we formally solve Eq. (D6) by using the Laplace transform

$$N_p(s) = \int_0^\infty dt N_p(t) e^{-st}.$$

When Eq. (D6) is rewritten in the image space, one can show that the function $N_p(s)$ has poles at

$$s - 2 \int_0^{\bar{\chi}_e} d\chi' \frac{dW_{\text{CS}}(\bar{\gamma}_e, \bar{\chi}_e, \chi')}{d\chi'} \frac{W_{\text{BW}}(\varepsilon', \chi')}{s + W_{\text{BW}}(\varepsilon', \chi')} = 0. \quad (\text{D7})$$

A positive solution $s_+ > 0$ of this equation provides the cascade growth rate in the steady state, $N_p(t) \simeq N_p(0)e^{\Gamma t}$, $\Gamma = s_+$. Eq. (D7) can be solved numerically. For more details, see Refs. [45, 63].

Equations (D6) and (D7) reproduce the model of Gris-mayer et al [see Eq. (9) in Ref. [45]]. It should be noted that in our derivation, we had to assume that the position of the electron spectrum coincides with $\bar{\varepsilon}_e$, namely, at the characteristic energy of the electron at the time of emission. This particular supposition (i) allowed decoupling f_\pm and $dW_{\text{rad}}/d\varepsilon_\gamma$ under the integral in Eq. (D3), and (ii) naturally cuts off the χ' -integral in Eq. (D7) at $\bar{\chi}_e$. However, our simulations show that for $\varepsilon_e \gtrsim \bar{\varepsilon}_e$ the spectrum decays exponentially, $f_\pm(\varepsilon_e, t) \propto \exp[-(\varepsilon_e/\bar{\varepsilon}_e)^n]$. Such behavior is expected as according to the initial hypothesis electrons emit photons as they reach such energies. Therefore, accounting for this feature may result in a refined version of Eq. (D7).

Let us point out here, that we demonstrated in Appendix C that Eqs. (18)-(19) for $N_{\pm, \gamma}(t)$ are *exact* in terms of the particle spectra, as we integrate them out without additional approximations (except the LCFA). The approximations that were applied in past works [40, 43, 46] and the new model that we propose in this work in Section III, also inexplicitly account for the particle spectrum precisely. The uncertainty of the mentioned models is contained in the approximation of $\bar{\varepsilon}_{e, \gamma}$, $\bar{\chi}_{e, \gamma}$, that are used to estimate the emission and pair creation rates.

Appendix E: Simulation setup

For the numerical study, we use the PIC code SMILEI [91] and perform simulations in the 1D3V geometry (1

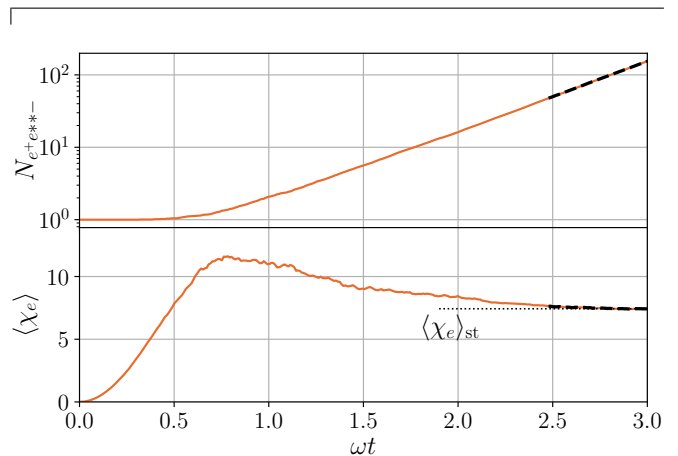


Figure 9. Example of one simulation in a rotating electric field. Top panel: the time dependence of the e^-e^+ pair number. Bottom panel: the average χ_e value of the electrons in the cascade. In the steady state, the growth rate Γ and $\langle \chi_e \rangle$ become stationary (see the corresponding horizontal line $\langle \chi_e \rangle_{\text{st}}$ in the bottom panel). The growth rate is extracted by using the exponential fitting of the dependence $N_{e^-e^+}(t) \propto e^{\Gamma t}$ at the data points depicted with the thick dashed line. The plot results from a simulation at $a_0 = 5275$.

spatial dimension in the direction transverse to the field and 3 momentum projections). The code consistently solves the equations of motion for particles and Maxwell's equations for EM fields, and includes the quantum processes of photon emission by electrons and positrons and pair creation by photons within the LCFA as given by Eqs. (2)-(5).

For the standing wave configuration, we pick the simulation box of length 4λ , and preliminary fill it with the field, so that the box is centered at the electric antinode. We initialize ≈ 100 seed electrons at rest in the vicinity of the center. The spatial and temporal resolution is set to $\lambda/128$ and $\min(T/500, T/a_0)$, respectively. We performed the convergence checks to validate the choice of temporal resolution. For the rotating field configuration, we use a 6λ simulation box. The field is prescribed by Eq. (10), and seed electrons are distributed in the middle 2λ -waist. For both configurations, we pick the initial electron density of $0.01n_c$, where $n_c = \varepsilon_0 m \omega^2 / e^2$ is the critical plasma density. Since our aim is testing the cascade growth model presented in Section III, we stay in the regime of relatively low particle densities when plasma effects are not significant (we discuss the field screening by the produced plasma in Section VII).

In addition, we performed several full 3D PIC simulations in a realistic configuration, when the standing wave

is formed by two focused Gaussian laser beams of circular polarization and with the waist $w_0 = 3\lambda$. The seeding conditions are the same as for the standing wave configuration, however, in this case, we start the simulation by injecting the beams from two opposite sides of an empty box, and seed electrons later, when the standing wave is formed. The EM field is calculated consistently in the PIC loop. We keep the total field amplitude at E_0 to match simulations in the other field configurations.

Extraction of the growth rate. In each simulation run, we observe an avalanche exhibiting exponential growth of the particle number, see an example in Fig. 9. We continue each run for a long enough time to ensure that the cascade reaches a steady state. The data collected in the steady state can be used to extract the growth rate Γ . The corresponding time points can be found by studying the time-dependence of the average electron Lorentz factor $\langle\gamma_e\rangle$ and χ -parameter $\langle\chi_e\rangle$. When the cascade reaches the steady state, $\langle\chi_e\rangle$ relaxes to the constant value $\langle\chi_e\rangle_{st}$, as illustrated in Fig. 9. Notably, the characteristic relaxation time depends on the field strength and decreases for higher E_0 . We select the steady-state time points by the following procedure: (i) equate value of $\langle\chi_e\rangle$ reached at the end of the simulation to $\langle\chi_e\rangle_{st}$, and (ii) pick time points from the data set tail that satisfy the condition $|\langle\chi_e\rangle(t) - \langle\chi_e\rangle_{st}|/\langle\chi_e\rangle_{st} < 0.02$. The growth rate Γ can be extracted by fitting the data for $N_{e^-e^+}(t)$ with the exponential function $A \exp(\Gamma t)$ for the selected points, where A and Γ are the fitting parameters.

Evaluation of the migration rate ν . Let us consider seed electrons in the field of a standing wave. If they are injected in spatial regions where $\chi_e(t)$ grows

fast, they can trigger a cascade. Recall that $\chi_e(t)$ is proportional to the value of $\epsilon^2\omega_{eff}$ [see Eq. (9)], which we plot in Fig. 4. It peaks in the electric node centers and rapidly falls off near the magnetic antinodes, where it vanishes. It is therefore beneficial to seed particles near the electric field peak, however, they will migrate to the magnetic antinodes, as the latter are spiraling attractors for charges [79, 80, 105–107]. Let us calculate the migration rate ν of e^-e^+ from the E -antinode center as a function of E_0 to evaluate its effect on the cascade growth rate.

The motion of an electron in a standing wave is known to be chaotic already in the classical regime. In our case, it is also affected by radiation. As general analytic expressions for the trajectories for this case are unknown, we perform statistical simulation of particle migration using SMILEI PIC code [91]. The simulation setup is the same as described above for the standing wave configuration, except that we seed $\sim 10^5$ macro-particles in the vicinity of the E -antinode and switch off pair creation for the photon species in the code, as we are interested particularly in the trajectories of the seed particles. Nevertheless, we fully account for the recoil due to photon emissions by the electrons. We define ν as the inverse time at which half of the particles propagate at distance $\lambda/8$ from the origin, meaning that they reach the spatial region where $\epsilon^2\omega_{eff} = 0$ (one of the shaded regions in Fig. 4). The resulting dependence $\nu(a_0)$ is presented in the bottom panel of Fig. 5. At low intensities, the migration rate is close to $\nu \approx T^{-1} = \omega/2\pi$, which is consistent with the analytical study in Ref. [106]. However as the amplitude grows, radiation effects become important and ν slowly decreases.

-
- [1] R. D. Blandford and R. L. Znajek, Electromagnetic extraction of energy from Kerr black holes, *MNRAS* **179**, 433 (1977).
 - [2] A. L. Ford, B. D. Keenan, and M. V. Medvedev, Electron-positron cascade in magnetospheres of spinning black holes, *Phys. Rev. D* **98**, 063016 (2018).
 - [3] F. C. Michel and H. Li, Electrodynamics of neutron stars, *Phys. Rep.* **318**, 227 (1999).
 - [4] P. Goldreich and W. H. Julian, Pulsar electrodynamics, *Astrophys. J.*, vol. 157, p. 869 **157**, 869 (1969).
 - [5] J. Arons, Some problems of pulsar physics or I'm madly in love with electricity, *Space Sci. Rev.* **24**, 437 (1979).
 - [6] R. Gueroult, Y. Shi, J.-M. Rax, and N. J. Fisch, Determining the rotation direction in pulsars, *Nat. Commun.* **10**, 3232 (2019).
 - [7] T. Piran, The physics of gamma-ray bursts, *Rev. Mod. Phys.* **76**, 1143 (2005).
 - [8] P. Chang, A. Spitkovsky, and J. Arons, Long-term evolution of magnetic turbulence in relativistic collisionless shocks: electron-positron plasmas, *Astrophys. J.* **674**, 378 (2008).
 - [9] A. Spitkovsky, Particle acceleration in relativistic collisionless shocks: Fermi process at last?, *Astrophys. J.* **682**, L5 (2008).
 - [10] P. Kumar and B. Zhang, The physics of gamma-ray bursts & relativistic jets, *Phys. Rep.* **561**, 1 (2015).
 - [11] A. N. Timokhin and A. K. Harding, On the maximum pair multiplicity of pulsar cascades, *Astrophys. J.* **871**, 12 (2019).
 - [12] F. Cruz, T. Grismayer, and L. O. Silva, Kinetic model of large-amplitude oscillations in neutron star pair cascades, *Astrophys. J.* **908**, 149 (2021).
 - [13] F. Cruz, T. Grismayer, S. Itanu, P. Tortone, and L. O. Silva, Model of pulsar pair cascades in non-uniform electric fields: Growth rate, density profile, and screening time, *Phys. Plasmas* **29**, <https://doi.org/10.1063/5.0085847> (2022).
 - [14] B. Cerutti, G. R. Werner, D. A. Uzdensky, and M. C. Begelman, Simulations of particle acceleration beyond the classical synchrotron burnoff limit in magnetic reconnection: an explanation of the Crab flares, *Astrophys. J.* **770**, 147 (2013).
 - [15] A. A. Philippov and A. Spitkovsky, Ab initio pulsar magnetosphere: three-dimensional particle-in-cell simulations of axisymmetric pulsars, *Astrophys. J. Lett.* **785**, L33 (2014).

- [16] R. Hu and A. M. Beloborodov, Axisymmetric pulsar magnetosphere revisited, *Astrophys. J.* **939**, 42 (2022).
- [17] H. Chen and F. Fiuza, Perspectives on relativistic electron–positron pair plasma experiments of astrophysical relevance using high-power lasers, *Phys. Plasmas* **30**, <https://doi.org/10.1063/5.0134819> (2023).
- [18] K. Qu, S. Meuren, and N. J. Fisch, Creating pair plasmas with observable collective effects, *Plasma Phys. Control. Fusion* **65**, 034007 (2023).
- [19] G. Sarri, K. Poder, J. Cole, W. Schumaker, A. Di Piazza, B. Reville, T. Dzelzainis, D. Doria, L. Gizzi, G. Grittani, *et al.*, Generation of neutral and high-density electron–positron pair plasmas in the laboratory, *Nat. Commun.* **6**, 6747 (2015a).
- [20] C. D. Arrowsmith, A. F. A. Bott, F. D. Cruz, D. H. Froula, *et al.*, Laboratory realization of relativistic pair-plasma beams, [arXiv preprint arXiv:2312.05244](https://arxiv.org/abs/2312.05244) (2023).
- [21] C. P. Ridgers, C. S. Brady, R. Duclous, J. G. Kirk, K. Bennett, T. D. Arber, and A. R. Bell, Dense electron-positron plasmas and bursts of gamma-rays from laser-generated quantum electrodynamic plasmas, *Phys. Plasmas* **20**, 056701 (2013).
- [22] N. B. Narozhny and A. M. Fedotov, Creation of electron-positron plasma with superstrong laser field, *Eur. Phys. J. Spec. Top.* **223**, 1083 (2014).
- [23] G. Sarri, M. E. Dieckmann, I. Kourakis, A. Di Piazza, B. Reville, C. Keitel, and M. Zepf, Overview of laser-driven generation of electron–positron beams, *J. Plasma Phys.* **81**, 455810401 (2015b).
- [24] P. Zhang, S. Bulanov, D. Seipt, A. V. Arefiev, and A. G. R. Thomas, Relativistic plasma physics in supercritical fields, *Phys. Plasmas* **27**, <https://doi.org/10.1063/1.5144449> (2020).
- [25] K. Qu, S. Meuren, and N. J. Fisch, Signature of collective plasma effects in beam-driven QED cascades, *Phys. Rev. Lett.* **127**, 095001 (2021).
- [26] A. Fedotov, A. Ilderton, F. Karbstein, B. King, D. Seipt, H. Taya, and G. Torgrimsson, Advances in QED with intense background fields, *Phys. Rep.* **1010**, 1 (2023).
- [27] A. Gonoskov, T. G. Blackburn, M. Marklund, and S. S. Bulanov, Charged particle motion and radiation in strong electromagnetic fields, *Rev. Mod. Phys.* **94**, 045001 (2022).
- [28] S. V. Popruzhenko and A. M. Fedotov, Dynamics and radiation of charged particles in ultra-intense laser fields, *Phys. Usp.* **66**, 460 (2023).
- [29] A. Di Piazza, C. Müller, K. Hatsagortsyan, and C. H. Keitel, Extremely high-intensity laser interactions with fundamental quantum systems, *Rev. Mod. Phys.* **84**, 1177 (2012).
- [30] R. Ruffini, G. Vereshchagin, and S.-S. Xue, Electron–positron pairs in physics and astrophysics: From heavy nuclei to black holes, *Phys. Rep.* **487**, 1 (2010).
- [31] T. K. Gaisser, R. Engel, and E. Resconi, *Cosmic rays and particle physics* (Cambridge University Press, Cambridge, 2016).
- [32] I. V. Sokolov, N. M. Naumova, J. A. Nees, and G. A. Mourou, Pair creation in QED-strong pulsed laser fields interacting with electron beams, *Phys. Rev. Lett.* **105**, 195005 (2010).
- [33] S. S. Bulanov, C. B. Schroeder, E. Esarey, and W. P. Leemans, Electromagnetic cascade in high-energy electron, positron, and photon interactions with intense laser pulses, *Phys. Rev. A* **87**, 062110 (2013).
- [34] T. Blackburn and C. Murphy, Scaling laws for positron production in laser–electron-beam collisions, *Phys. Rev. A* **96**, 022128 (2017).
- [35] A. Mercuri-Baron, M. Grech, F. Niel, A. Grassi, M. Lobet, A. Di Piazza, and C. Riconda, Impact of the laser spatio-temporal shape on Breit–Wheeler pair production, *New J. Phys.* **23**, 085006 (2021).
- [36] C. D. Zerby and H. S. Moran, Studies of the longitudinal development of electron–photon cascade showers, *J. Appl. Phys.* **34**, 2445 (1963).
- [37] V. I. Ritus, Quantum effects of the interaction of elementary particles with an intense electromagnetic field, *J. Russ. Laser Res.* **6**, 497 (1985).
- [38] A. R. Bell and J. G. Kirk, Possibility of prolific pair production with high-power lasers, *Phys. Rev. Lett.* **101**, 200403 (2008).
- [39] J. G. Kirk, A. R. Bell, and I. Arka, Pair production in counter-propagating laser beams, *Plasma Phys. Control. Fusion* **51**, 085008 (2009).
- [40] A. M. Fedotov, N. B. Narozhny, G. Mourou, and G. Korn, Limitations on the attainable intensity of high power lasers, *Phys. Rev. Lett.* **105**, 080402 (2010).
- [41] A. Gonoskov, A. Bashinov, S. Bastrakov, E. Efimenko, A. Ilderton, A. Kim, M. Marklund, I. Meyerov, A. Muraviev, and A. Sergeev, Ultrabright gev photon source via controlled electromagnetic cascades in laser-dipole waves, *Phys. Rev. X* **7**, 041003 (2017).
- [42] A. A. Mironov, E. G. Gelfer, and A. M. Fedotov, Onset of electron-seeded cascades in generic electromagnetic fields, *Phys. Rev. A* **104**, 012221 (2021).
- [43] N. V. Elkina, A. M. Fedotov, I. Y. Kostyukov, M. V. Legkov, N. B. Narozhny, E. N. Nerush, and H. Ruhl, QED cascades induced by circularly polarized laser fields, *Phys. Rev. STAB* **14**, 054401 (2011).
- [44] A. A. Mironov, N. B. Narozhny, and A. M. Fedotov, Collapse and revival of electromagnetic cascades in focused intense laser pulses, *Phys. Lett. A* **378**, 3254 (2014).
- [45] T. Grismayer, M. Vranic, J. L. Martins, R. A. Fonseca, and L. O. Silva, Seeded QED cascades in counterpropagating laser pulses, *Phys. Rev. E* **95**, 023210 (2017).
- [46] V. F. Bashmakov, E. N. Nerush, I. Y. Kostyukov, A. M. Fedotov, and N. B. Narozhny, Effect of laser polarization on quantum electrodynamical cascading, *Phys. Plasmas* **21**, 013105 (2014).
- [47] M. Jirka, O. Klimo, S. V. Bulanov, T. Z. Esirkepov, E. Gelfer, S. S. Bulanov, S. Weber, and G. Korn, Electron dynamics and γ and e^-e^+ production by colliding laser pulses, *Phys. Rev. E* **93**, 023207 (2016).
- [48] E. G. Gelfer, A. A. Mironov, A. M. Fedotov, V. F. Bashmakov, E. N. Nerush, I. Y. Kostyukov, and N. B. Narozhny, Optimized multibeam configuration for observation of QED cascades, *Phys. Rev. A* **92**, 022113 (2015).
- [49] M. Marklund, T. G. Blackburn, A. Gonoskov, J. Magnusson, S. S. Bulanov, and A. Ilderton, Towards critical and supercritical electromagnetic fields, *High Power Laser Sci. Eng.* **11**, e19 (2023).
- [50] H. Vincenti, T. Clark, L. Fedeli, P. Martin, A. Sainte-Marie, and N. Zaim, Plasma mirrors as a path to the Schwinger limit: theoretical and numerical developments, *Eur. Phys. J.: Spec. Top.* **232**, 2303 (2023).
- [51] C. P. Ridgers, C. S. Brady, R. Duclous, J. G. Kirk, K. Bennett, T. D. Arber, A. P. L. Robinson, and A. R. Bell, Dense electron-positron plasmas and ultraintense

- γ rays from laser-irradiated solids, *Phys. Rev. Lett.* **108**, 165006 (2012).
- [52] M. Jirka, O. Klimo, M. Vranic, S. Weber, and G. Korn, QED cascade with 10 PW-class lasers, *Sci. Rep.* **7**, 15302 (2017).
- [53] C. Slade-Lowther, D. D. Sorbo, and C. P. Ridgers, Identifying the electron–positron cascade regimes in high-intensity laser-matter interactions, *New J. Phys.* **21**, 013028 (2019).
- [54] X.-L. Zhu, T.-P. Yu, Z.-M. Sheng, Y. Yin, I. C. E. Turcu, and A. Pukhov, Dense GeV electron–positron pairs generated by lasers in near-critical-density plasmas, *Nat. Commun.* **7**, <https://doi.org/10.1038/ncomms13686> (2016).
- [55] A. S. Samsonov, I. Y. Kostyukov, and E. N. Nerush, Hydrodynamical model of QED cascade expansion in an extremely strong laser pulse, *Matter Radiat. Extremes* **6**, <https://doi.org/10.1063/5.0035347> (2021).
- [56] I. I. Artemenko and I. Y. Kostyukov, Ionization-induced laser-driven QED cascade in noble gases, *Phys. Rev. A* **96**, 032106 (2017).
- [57] M. Tamburini, A. Di Piazza, and C. H. Keitel, Laser-pulse-shape control of seeded QED cascades, *Sci. Rep.* **7**, <http://doi.org/10.1038/s41598-017-05891-z> (2017).
- [58] M. Jirka and S. Bulanov, Effects of colliding laser pulses polarization on e^-e^+ cascade development in extreme focusing, *arXiv preprint arXiv:2401.08410* (2024).
- [59] M. Lobet, C. Ruyer, A. Debayle, E. d’Humières, M. Grech, M. Lemoine, and L. Gremillet, Ultrafast synchrotron-enhanced thermalization of laser-driven colliding pair plasmas, *Phys. Rev. Lett.* **115**, 215003 (2015).
- [60] J. Y. Yu, T. Yuan, W. Y. Liu, M. Chen, W. Luo, S. M. Weng, and Z. M. Sheng, QED effects induced harmonics generation in extreme intense laser foil interaction, *Plasma Phys. Control. Fusion* **60**, 044011 (2018).
- [61] W. Luo, W.-Y. Liu, T. Yuan, M. Chen, J.-Y. Yu, F.-Y. Li, D. Del Sorbo, C. P. Ridgers, and Z.-M. Sheng, QED cascade saturation in extreme high fields, *Sci. Rep.* **8**, 8400 (2018).
- [62] E. N. Nerush, V. F. Bashmakov, and I. Y. Kostyukov, Analytical model for electromagnetic cascades in rotating electric field, *Phys. Plasmas* **18**, 083107 (2011).
- [63] T. Grismayer, M. Vranic, J. L. Martins, R. A. Fonseca, and L. O. Silva, Laser absorption via quantum electrodynamics cascades in counter propagating laser pulses, *Phys. Plasmas* **23**, 056706 (2016).
- [64] E. S. Efimenko, A. V. Bashinov, S. I. Bastrakov, A. A. Gonoskov, A. A. Muraviev, I. B. Meyerov, A. V. Kim, and A. M. Sergeev, Extreme plasma states in laser-governed vacuum breakdown, *Sci. Rep.* **8**, 2329 (2018).
- [65] D. Papadopoulos, J.-P. Zou, C. Le Blanc, L. Ranc, F. Druon, L. Martin, A. Fréneaux, A. Beluze, N. Lebas, M. Chabanis, *et al.*, First commissioning results of the apollon laser on the 1 PW beam line, in *CLEO: Science and Innovations* (Optica Publishing Group, 2019) pp. STu3E–4.
- [66] S. Weber, S. Bechet, S. Borneis, L. Brabec, M. Bučka, E. Chacon-Golcher, M. Ciappina, M. DeMarco, A. Fajstavr, K. Falk, *et al.*, P3: An installation for high-energy density plasma physics and ultra-high intensity laser–matter interaction at ELI-Beamlines, *Matter Radiat. at Extremes* **2**, 149 (2017).
- [67] Center for Relativistic Laser Science, https://corels.ibs.re.kr/html/corels_en/.
- [68] K. A. Tanaka, K. M. Spohr, D. L. Balabanski, S. Balascuta, L. Capponi, M. O. Cernaianu, M. Cuciuc, A. Cuciocanes, I. Dancus, A. Dhal, *et al.*, Current status and highlights of the ELI-NP research program, *Matter Radiat. at Extremes* **5**, 024402 (2020).
- [69] Astra Gemini laser, <https://www.clf.stfc.ac.uk/Pages/The-Astra-Gemini-Facility.aspx>.
- [70] Z. Gan, L. Yu, S. Li, C. Wang, X. Liang, Y. Liu, W. Li, Z. Guo, Z. Fan, X. Yuan, *et al.*, 200 J high efficiency Ti:sapphire chirped pulse amplifier pumped by temporal dual-pulse, *Opt. Express* **25**, 5169 (2017).
- [71] PEARL laser complex, <https://ipfran.ru/science/laser-physics-and-nonlinear-optics/generation-of-extreme-laser-fields/PEARL-laser-complex>.
- [72] C. N. Danson, C. Haefner, J. Bromage, T. Butcher, J.-C. F. Chanteloup, E. A. Chowdhury, A. Galvanauskas, L. A. Gizzi, J. Hein, D. I. Hillier, *et al.*, Petawatt and exawatt class lasers worldwide, *High Power Laser Sci. Eng.* **7**, <https://doi.org/10.1017/hpl.2019.36> (2019).
- [73] J. W. Yoon, Y. G. Kim, I. W. Choi, J. H. Sung, H. W. Lee, S. K. Lee, and C. H. Nam, Realization of laser intensity over 10^{23} W/cm², *Optica* **8**, 630 (2021).
- [74] J. Bromage, S.-W. Bahk, I. A. Begishev, C. Dorrer, M. J. Guardalben, B. N. Hoffman, J. B. Oliver, R. G. Roides, E. M. Schiesser, M. J. Shoup Iii, *et al.*, Technology development for ultraintense all-OPCPA systems, *High Power Laser Sci. Eng.* **7**, e4 (2019).
- [75] NSF OPAL, <https://www.lle.rochester.edu/nsf-opal/>.
- [76] E. Khazanov, A. Shaykin, I. Kostyukov, V. Ginzburg, I. Mukhin, I. Yakovlev, A. Soloviev, I. Kuznetsov, S. Mironov, A. Korzhimantov, *et al.*, eXawatt Center for Extreme Light Studies, *High Power Laser Sci. Eng.* **11**, e78 (2023).
- [77] B. Shao, Y. Li, Y. Peng, P. Wang, J. Qian, Y. Leng, and R. Li, Broad-bandwidth high-temporal-contrast carrier-envelope-phase-stabilized laser seed for 100 PW lasers, *Optics Lett.* **45**, 2215 (2020).
- [78] I. Y. Kostyukov, I. I. Artemenko, and E. N. Nerush, Growth rate of QED cascades in a rotating electric field, *Probl. At. Sci. Technol.*, 259 (2018).
- [79] T. Z. Esirkepov, S. S. Bulanov, J. K. Koga, M. Kando, K. Kondo, N. N. Rosanov, G. Korn, and S. V. Bulanov, Attractors and chaos of electron dynamics in electromagnetic standing waves, *Phys. Lett. A* **379**, 2044 (2015).
- [80] B. King and H. Hu, Classical and quantum dynamics of a charged scalar particle in a background of two counterpropagating plane waves, *Phys. Rev. D* **94**, 125010 (2016).
- [81] F. Niel, C. Riconda, F. Amiranoff, R. Ducloux, and M. Grech, From quantum to classical modeling of radiation reaction: A focus on stochasticity effects, *Phys. Rev. E* **97**, 043209 (2018).
- [82] G. Fauth, J. Berges, and A. Di Piazza, Collisional strong-field QED kinetic equations from first principles, *Phys. Rev. D* **104**, 036007 (2021).
- [83] A. Gonoskov, S. Bastrakov, E. Efimenko, A. Ilderton, M. Marklund, I. Meyerov, A. Muraviev, A. Sergeev, I. Surmin, and E. Wallin, Extended particle-in-cell schemes for physics in ultrastrong laser fields: Review and developments, *Phys. Rev. E* **92**, 023305 (2015).

- [84] B. King, N. Elkina, and H. Ruhl, Photon polarization in electron-seeded pair-creation cascades, *Phys. Rev. A* **87**, 042117 (2013).
- [85] D. Seipt and A. G. R. Thomas, Kinetic theory for spin-polarized relativistic plasmas, *Phys. Plasmas* **30**, <https://doi.org/10.1063/5.0165836> (2023).
- [86] Q. Zhao, T. Sun, K. Xue, F. Wan, and J.-X. Li, Cascade of polarized Compton scattering and Breit-Wheeler pair production, *Phys. Rev. D* **108**, 116012 (2023).
- [87] A. Sampath and M. Tamburini, Towards realistic simulations of QED cascades: Non-ideal laser and electron seeding effects, *Phys. Plasmas* **25**, <https://doi.org/10.1063/1.5022640> (2018).
- [88] M. Jirka, P. Satorov, S. S. Bulanov, G. Korn, B. Rus, and S. V. Bulanov, Reaching high laser intensity by a radiating electron, *Phys. Rev. A* **103**, 053114 (2021a).
- [89] A. A. Mironov, A. M. Fedotov, and N. B. Narozhny, Generation of quantum-electrodynamic cascades in oblique collisions of ultrarelativistic electrons with an intense laser field, *Quantum Electron.* **46**, 305 (2016).
- [90] S. S. Bulanov, V. D. Mur, N. B. Narozhny, J. Nees, and V. S. Popov, Multiple colliding electromagnetic pulses: a way to lower the threshold of e^+e^- pair production from vacuum, *Phys. Rev. Lett.* **104**, 220404 (2010).
- [91] J. Derouillat, A. Beck, F. Pérez, T. Vinci, M. Chiaramello, A. Grassi, M. Flé, G. Bouchard, I. Plotnikov, N. Aunai, *et al.*, Smilei: A collaborative, open-source, multi-purpose particle-in-cell code for plasma simulation, *Comp. Phys. Comm.* **222**, 351 (2018).
- [92] A. I. Nikishov and V. I. Ritus, Quantum processes in the field of a plane electromagnetic wave and in a constant field I, *Sov. Phys. JETP* **19**, 529 (1964).
- [93] A. I. Nikishov and V. I. Ritus, Pair production by a photon and photon emission by an electron in the field of an intense electromagnetic wave and in a constant field, *Sov. Phys. JETP* **25**, 1135 (1967).
- [94] V. N. Baier and V. M. Katkov, Processes involved in the motion of high energy particles in a magnetic field, *Sov. Phys. JETP* **26**, 854 (1968).
- [95] E. G. Gelfer, A. M. Fedotov, A. A. Mironov, and S. Weber, Nonlinear Compton scattering in time-dependent electric fields beyond the locally constant crossed field approximation, *Phys. Rev. D* **106**, 056013 (2022).
- [96] A. Di Piazza, M. Tamburini, S. Meuren, and C. H. Keitel, Implementing nonlinear Compton scattering beyond the local-constant-field approximation, *Phys. Rev. A* **98**, 012134 (2018).
- [97] A. Di Piazza and S. Meuren, Improved local-constant-field approximation for strong-field QED codes, *Phys. Rev. A* **99**, 022125 (2019).
- [98] A. Ilderton, B. King, and D. Seipt, Extended locally constant field approximation for nonlinear Compton scattering, *Phys. Rev. A* **99**, 042121 (2019).
- [99] E. Raicher, S. Eliezer, C. H. Keitel, and K. Z. Hatsagortsyan, Semiclassical limitations for photon emission in strong external fields, *Phys. Rev. A* **99**, 052513 (2019).
- [100] T. Heinzl, B. King, and A. J. MacLeod, Locally monochromatic approximation to QED in intense laser fields, *Phys. Rev. A* **102**, 063110 (2020).
- [101] B. King, Uniform locally constant field approximation for photon-seeded pair production, *Phys. Rev. A* **101**, 042508 (2020).
- [102] A. Di Piazza, WKB electron wave functions in a tightly focused laser beam, *Phys. Rev. D* **103**, 076011 (2021).
- [103] C. F. Nielsen, R. Holtzapple, and B. King, High-resolution modeling of nonlinear Compton scattering in focused laser pulses, *Phys. Rev. D* **106**, 013010 (2022).
- [104] A. H. Taub, Orbits of charged particles in constant fields, *Phys. Rev.* **73**, 786 (1948).
- [105] G. Lehmann and K. H. Spatschek, Phase-space contraction and attractors for ultrarelativistic electrons, *Phys. Rev. E* **85**, 056412 (2012).
- [106] Z. Gong, R. Hu, Y. Shou, B. Qiao, C. Chen, F. Xu, X. He, and X. Yan, Radiation reaction induced spiral attractors in ultra-intense colliding laser beams, *Matter Radiat. Extremes* **1**, 308 (2016).
- [107] J. G. Kirk, Radiative trapping in intense laser beams, *Plasma Phys. Control. Fusion* **58**, 085005 (2016).
- [108] M. Jirka, O. Klimo, and M. Matys, Relativistic plasma aperture for laser intensity enhancement, *Phys. Rev. R* **3**, 033175 (2021b).
- [109] A. Gonoskov, A. Bashinov, I. Gonoskov, C. Harvey, A. Ilderton, A. Kim, M. Marklund, G. Mourou, and A. Sergeev, Anomalous radiative trapping in laser fields of extreme intensity, *Phys. Rev. Lett.* **113**, 014801 (2014).
- [110] A. V. Bashinov, E. S. Efimenko, A. A. Muraviev, V. D. Volokitin, I. B. Meyerov, G. Leuchs, A. M. Sergeev, and A. V. Kim, Particle trajectories, gamma-ray emission, and anomalous radiative trapping effects in magnetic dipole wave, *Phys. Rev. E* **105**, 065202 (2022).